

# Spatial and Binary Parameter Distributions of Black Hole Binaries in the Milky Way Detectable with *Gaia*

MINORI SHIKAUCHI,<sup>1,2,3</sup> DAICHI TSUNA,<sup>4,2</sup> ATARU TANIKAWA,<sup>5</sup> AND NORITA KAWANAKA<sup>6</sup>

<sup>1</sup>*Department of Physics, the University of Tokyo, 7-3-1 Hongo, Bunkyo, Tokyo 113-0033, Japan*

<sup>2</sup>*Research Center for the Early Universe (RESCEU), the University of Tokyo, 7-3-1 Hongo, Bunkyo, Tokyo 113-0033, Japan*

<sup>3</sup>*Department of Physics and Astronomy, the University of British Columbia, 6224 Agricultural Road, Vancouver, BC, V6T 1Z1, Canada*

<sup>4</sup>*TAPIR, Mailcode 350-17, California Institute of Technology, Pasadena, CA 91125, USA*

<sup>5</sup>*Department of Earth Science and Astronomy, College of Arts and Sciences, the University of Tokyo, 3-8-1 Komaba, Meguro, Tokyo 153-8902, Japan*

<sup>6</sup>*Center for Gravitational Physics and Quantum Information, Yukawa Institute for Theoretical Physics, Kyoto University, Kitashirakawa Oiwake-cho, Sakyo-ku, Kyoto, 606-8502, Japan*

(Received January 16, 2022)

## ABSTRACT

Soon after the *Gaia* data release (DR) 3 in June 2022, some candidates (and one confirmed) of detached black hole (BH) - luminous companion (LC) binaries have been reported. Existing and future detections of astrometric BH-LC binaries will shed light on the spatial distribution of these systems, which can deepen our understanding of the natal kicks and the underlying formation mechanism of BHs. By tracking Galactic orbits of BH-LC binaries obtained from BSE, we find that distributions of BH mass and the height from the Galactic plane  $|z|$  would help us give a constraint on supernova model. We also indicate that the correlations of (i) orbital periods and eccentricities, and (ii) BH mass and  $|z|$  could be clues for the strength of natal kick. We also discuss the possibility of forming BH-LC binaries like the BH binary candidates reported in *Gaia* DR3 and *Gaia* BH 1, finding that if the candidates as well as the confirmed binary originate from isolated binaries, they favor models which produce low-mass BHs and have high common envelope efficiencies exceeding unity.

*Keywords:* astrometry — stars: black holes — binaries: general

## 1. INTRODUCTION

Massive stars are often formed in binaries, which can leave behind compact objects including black holes (BHs) after core-collapse. Such BHs in binary systems are important tools for probing how BHs are born and evolve, as well as the uncertainties of binary evolution models. By observing sinusoidal motions of luminous companions (LCs), the astrometric satellite *Gaia* (Esa 1997) is supposed to detect non-interacting binaries consisting of LCs and unseen objects, and estimate the mass of the unseen object. If the unseen object mass is larger than a few solar masses and we do not find any excess emission from them by spectroscopy or photometry, the unseen object should be BHs. Since *Gaia* has been observing for more than five years, orbital periods of the detectable binaries with *Gaia* should be tens of days to several years, longer than observed in BH X-ray binaries (XRBs). Observations of low mass XRBs (LMXBs) imply the absence of  $3 - 5M_{\odot}$  BHs (Özel et al. 2010; Farr et al. 2011), so-called lower mass gap (Bailyn et al. 1998). However, *Gaia* might reveal a completely different BH population from X-ray binaries, and thus has been attracting more and more people's interest.

There are an increasing number of papers that assess *Gaia*'s detectability of BH-LC binaries (*e.g.* Mashian & Loeb 2017; Breivik et al. 2017; Yamaguchi et al. 2018; Kinugawa & Yamaguchi 2018; Yalinewich et al. 2018; Andrews et al. 2019; Shao & Li 2019; Wiktorowicz et al. 2020; Shikauchi et al. 2020; Chawla et al. 2021; Shikauchi et al. 2022). *Gaia*

should be able to detect several to thousands of BH-LC binaries in the five-year mission. The detectability is greatly dependent on some factors such as binary evolution models (Breivik et al. 2017; Chawla et al. 2021; Shikauchi et al. 2022) and detection criteria adopted in each work.

The recent data release (Data release 3, DR3) was on June 13, 2022 <sup>1</sup>, which provided about  $3.3 \times 10^7$  additional sources from DR2 and the information of  $8.1 \times 10^5$  non-single stars, *e.g.* binaries, from its data spanning about three years. The *Gaia* collaboration reported BH-main sequence (MS) or post-MS star binary candidates from its spectroscopic data (Gaia Collaboration et al. 2022; Gomel et al. 2022), which were however rejected by El-Badry & Rix (2022) to possess BHs for all of the BH-MS star candidates. More recently, El-Badry et al. (2023) identified *Gaia* DR3 4373465352415301632 as a binary consisting of a BH and a G dwarf star, and additional BH-LC binary candidates were reported in independent works (Andrews et al. 2022; Shahaf et al. 2022; Tanikawa et al. 2022). As the number of detections increases in the near future, the distributions of the binary parameters, such as the orbital parameters and locations in the Milky Way (MW) phase-space, would be uncovered. Such distributions should reflect the effect of BH natal kicks that accompany the core-collapse of the BHs' progenitors.

Studies on spatial distributions of BHs have already been done for XRBs (Gandhi et al. 2020; Jonker et al. 2021). Analogous to BH XRBs, the spatial distribution of BH binary candidates reported in *Gaia* DR3 may pose an independent constraint on BH natal kick models and their origin, as the *Gaia*-detectable BH-LC binaries are supposed to have longer orbital periods than BH XRBs.

In this work, we investigate the spatial distribution of BH-LC binaries detectable with *Gaia*, by obtaining BH-LC binary population with the binary population synthesis code and tracking their motions under the MW potential. In section 2, we describe the initial spatial condition employed here and the initial set-up for the binary population synthesis code, and explain how to simulate the orbits of BH-LC binaries in the MW from formation to the present day. We show the results in section 3 and compare our samples with the reported BH candidates in section 4. Our conclusion is in section 5.

## 2. METHOD

In this section, we summarize the initial spatial condition in subsection 2.1. The binary population synthesis code and binary evolution models that we employ are depicted in subsection 2.2. How we track the motion of BH-LC binaries under the MW potential is described in subsection 2.3. We also explain sampling techniques to conduct our simulation efficiently in subsection 2.4. Finally, the detection criteria with *Gaia* that are employed in this work are summarized in subsection 2.5.

### 2.1. Initial Conditions with Configuration of the MW

Here, we follow Wagg et al. (2021) to synthesize the binary populations throughout the history of the MW. The formalism of Wagg et al. (2021) is based on an empirically-informed analytic model that adopts the metallicity-radius-time relations in Frankel et al. (2018). The relations were calibrated based on data of red clump stars observed with APOGEE (Majewski et al. 2017).

The MW model consists of three components: the low- $[\alpha/\text{Fe}]$  disc (*i.e.* the thin disc), the high- $[\alpha/\text{Fe}]$  disc (*i.e.* the thick disc) and the bar/bulge-like central component. The double disc model reasonably explains the stellar distribution in the MW. For the three components, star formation history and the spatial distribution are modelled independently. For the star-formation history, we weight each model based on the current stellar mass of each component as follows. Assuming that the stellar mass of the bulge  $M_{\text{bulge}}$  is  $0.9 \times 10^{10} M_{\odot}$ , that of both disc components  $M_{\text{disc}}$  is  $5.2 \times 10^{10} M_{\odot}$  (Licquia & Newman 2015), and the masses of the thin and thick discs are equal (e.g. Snaith et al. 2014), the number of simulated initial binaries in each component,  $N_{\text{thin}}$  in the thin disc,  $N_{\text{thick}}$  in the thick disc, and  $N_{\text{bulge}}$  in the bulge are

$$N_i = N \times \int_0^{\tau_m} \frac{p(\tau)}{M_{\text{tot}}} d\tau, \quad (1)$$

$$= \begin{cases} N \times \frac{M_{\text{disc}}/2}{M_{\text{tot}}} & (\text{the thin/thick disc}), \\ N \times \frac{M_{\text{bulge}}}{M_{\text{tot}}} & (\text{the bulge}), \end{cases} \quad (2)$$

<sup>1</sup> <https://www.cosmos.esa.int/web/gaia/data-release-3>

where the suffix *i* represents each component in the MW (*i.e.*, the thin/thick disc and the bulge component),  $N = 10^7$  is the total number of initial binaries in one realization, and  $M_{\text{tot}} = M_{\text{disc}} + M_{\text{bulge}}$ .

For the disc components, the star formation history  $p(\tau)$  can be shown as an exponential form,

$$p(\tau)d\tau \propto \exp\left(-\frac{\tau_m - \tau}{\tau_{\text{SFR}}}\right) d\tau, \quad (3)$$

where  $\tau$  is the lookback time, *i.e.* the time elapsed from a binary stars' zero-age MS (ZAMS) stage to now,  $\tau_m = 12$  Gyr is the age of the MW, and  $\tau_{\text{SFR}}$  is a timescale of the star formation, 6.8 Gyr, based on Frankel et al. (2018). Note that the periods of star formation in the two discs are different, and stars are formed earlier in the thick disc ( $\tau = 8 - 12$  Gyr) and later in the thin disc ( $\tau = 0 - 8$  Gyr). For the bulge component, considering that the central bars seem to include stars with ages of 6 - 12 Gyr with a tail of younger ages and that there are uncertainties on its star formation history, we adopt a scaled and shifted version of the beta function expressed below.

In summary, the exact expression of the star formation history  $p(\tau)$  including normalization factors is

$$p(\tau)d\tau = \begin{cases} \frac{M_{\text{disc}}}{2M_{\text{tot}}} \times n_{\text{thin}} \exp\left(-\frac{\tau_m - \tau}{\tau_{\text{SFR}}}\right) d\tau & \text{(the thin disc, } 0 \text{ Gyr} < \tau < 8 \text{ Gyr)}, \\ \frac{M_{\text{disc}}}{2M_{\text{tot}}} \times n_{\text{thick}} \exp\left(-\frac{\tau_m - \tau}{\tau_{\text{SFR}}}\right) d\tau & \text{(the thick disc, } 8 \text{ Gyr} < \tau < 12 \text{ Gyr)}, \\ \frac{M_{\text{bulge}}}{M_{\text{tot}}} \times \beta(2, 3)(\tau') d\tau & \text{(the bulge, } 6 \text{ Gyr} < \tau < 12 \text{ Gyr)}, \end{cases} \quad (4)$$

where

$$\begin{cases} n_{\text{thin}} = \frac{1}{\int_{\tau=0}^{8 \text{ Gyr}} \exp\left(-\frac{\tau_m - \tau}{\tau_{\text{SFR}}}\right) d\tau}, \\ n_{\text{thick}} = \frac{1}{\int_{\tau=8 \text{ Gyr}}^{12 \text{ Gyr}} \exp\left(-\frac{\tau_m - \tau}{\tau_{\text{SFR}}}\right) d\tau}, \end{cases} \quad (5)$$

and  $\beta(2, 3)(\tau')$  is the beta function,

$$\beta(2, 3)(\tau') = \frac{\Gamma(5) \times \tau'(1 - \tau')^2}{\Gamma(2)\Gamma(3)}, \quad (6)$$

where  $\tau' = (\tau/6 \text{ Gyr}) - 1$  so that the beta function is scaled and shifted as  $\beta = 0$  at  $\tau = 6$  Gyr, 12 Gyr with  $\Gamma$ , the Gamma function.

Then, we distribute the initial binaries following the radial and the vertical distributions shown below. For the radial distribution, a single exponential distribution is employed,

$$q(R)dR = \exp\left(-\frac{R}{R_d}\right) \frac{R}{R_d^2} dR, \quad (7)$$

where  $R$  is a radius from the Galactic center, and  $R_d$  is a scale length. For the thin disc,  $R_d$  is defined as

$$R_d \equiv R_{\text{exp}}(\tau) = 4 \text{ kpc} \left(1 - \alpha_{R_{\text{exp}}} \left(\frac{\tau}{8 \text{ Gyr}}\right)\right), \quad (8)$$

where  $\alpha_{R_{\text{exp}}} = 0.3$  as the inside-out growth parameter. For the thick disc and the bar structure,  $R_d$  is age-independent with the respective values (1/0.43) kpc (Table 1, Bovy et al. 2019) and 1.5 kpc (Bovy et al. 2019).

The vertical distribution for each component is a single exponential form as well,

$$s(|z|)dz = \frac{1}{z_d} \exp\left(-\frac{z}{z_d}\right) dz, \quad (9)$$

where  $z$  is a height from the Galactic plane and  $z_d$  is a scale height. The value of  $z_d$  for each component is 0.3 kpc for the thin disc (McMillan 2011), 0.95 kpc for the thick disc (Bovy et al. 2019), and 0.2 kpc for the bulge component (Wegg et al. 2015).

Finally, the metallicity of each star is given as a function of radius and lookback time,

$$[\text{Fe}/\text{H}](R, \tau) = F_m + \nabla[\text{Fe}/\text{H}]R - \left(F_m + \nabla[\text{Fe}/\text{H}]R_{[\text{Fe}/\text{H}] = 0}^{\text{now}}\right) f(\tau), \quad (10)$$

where

$$f(\tau) = \left(1 - \frac{\tau}{\tau_m}\right)^{\gamma_{[\text{Fe}/\text{H}]}} , \quad (11)$$

$F_m = -1$  dex is the metallicity of the star-forming gas at the center of the disc at  $\tau = \tau_m$ ,  $\nabla[\text{Fe}/\text{H}] = -0.075 \text{ kpc}^{-1}$  is the metallicity gradient, and  $R_{[\text{Fe}/\text{H}]=0}^{\text{now}} = 8.7 \text{ kpc}$  is the radius at which the present metallicity is the solar value  $Z_\odot = 0.014$ . The value  $\gamma_{[\text{Fe}/\text{H}]} = 0.3$  accounts for the time-dependence of the chemical enrichment. The metallicity can then be obtained by the relation below (e.g. Bertelli et al. 1994),

$$\log_{10}(Z) = 0.977[\text{Fe}/\text{H}] + \log_{10}(Z_\odot). \quad (12)$$

We note that Wagg et al. (2021) applied this conversion to the thick disc and the bulge component as well as the thin disc, although Frankel et al. (2018) fitted this model only for stars in the thin disc.

To convert the number of BH-LC binaries obtained in the simulation  $N_{\text{BH-LC, sim}}$  to the actual number in the MW  $N_{\text{BH-LC, MW}}$ ,

$$N_{\text{BH-LC, MW}} = N_{\text{BH-LC, sim}} \times \frac{M_{\text{tot}}}{M_{\text{tot, sim}}}, \quad (13)$$

where  $M_{\text{tot, sim}}$  is the total initial mass in the simulation. Note that we restrict the initial primary mass  $m_{\text{prim, ZAMS}}$  to be from  $8M_\odot$ . The value  $M_{\text{tot, sim}}$  is thus corrected to the actual total mass with  $m_{\text{prim, ZAMS}} \geq 0.08M_\odot$ , using the initial primary mass function described below. We assume the binary fraction as unity since the value with O-type stars is estimated as  $\sim 0.7$  in Sana et al. (2012). A lower value of the binary fraction will shift down the overall number of detectable binaries, but will not affect the correlations between the parameters studied in section 3.

## 2.2. Binary Population Synthesis Code and Binary Evolution Models

Binary evolution is simulated by the binary population synthesis code BSE (Hurley et al. 2000; Hurley et al. 2002). We update the stellar wind model in BSE to a metallicity-dependent one following Belczynski et al. (2010).

Two different supernova (SN) mechanisms are employed: “rapid” and “delayed” models suggested in Fryer et al. (2012). In the rapid model, BHs as light as  $2 - 4.5M_\odot$  are rarely born, which reproduces the lower BH mass gap in X-ray observations (Özel et al. 2010; Farr et al. 2011). Meanwhile, such “mass gap” BHs can be formed in the delayed model. We use both SN models, as it is still uncertain whether the mass gap is intrinsic or due to observational bias.

We also adopt “fallback (FB) kick” model (Fryer et al. 2012) for the rapid and the delayed SN models as BH natal kicks. The strength of BH natal kicks is that of neutron star (NS) natal kicks modulated by  $(1 - f_{\text{fb}})$ , where  $f_{\text{fb}}$  is the fraction of fallback matter to the ejected mass. The distribution of NS kicks is supposed to be Maxwellian distribution with  $\sigma = 265 \text{ km s}^{-1}$  (Hobbs et al. 2005). In general, the mass of the remnant BH tends to be larger in the rapid model than in the delayed model, so the magnitude of FB kick in the rapid model is negligible. In order to see the effect of FB kick, we employ a model with no FB kick for the delayed model as a comparison. We note that there is also contribution of kick from rapid mass loss upon core-collapse (Blaauw kick; Blaauw 1961), which are included in all of the models.

While the common envelope (CE) phase is treated by  $\alpha\lambda$  prescription (equation 3 in Ivanova et al. 2013), two different CE efficiencies,  $\alpha = 1$  and  $10$  are employed. The latter choice is motivated by El-Badry et al. (2023), which indicated that *Gaia* BH 1 cannot be formed with  $\alpha = 1$  under the assumption of isolated binary origin, and Hirai & Mandel (2022), which revealed that under their new CE formalism post-CE separations can get as large as those translating to a high CE efficiency reaching  $\alpha = 10$ . We apply the result in Claeys et al. (2014) for  $\lambda$ .

For the distributions of initial binary parameters, we assume a single initial primary mass function of Kroupa (2001) from  $8M_\odot$  to  $150M_\odot$ . The mass ratio is assumed to be flat from  $0.1/m_{\text{prim, ZAMS}}$  to  $1$  (Kuiper 1935; Kobulnicky & Fryer 2007). The minimum value of the initial secondary mass is set to  $0.1M_\odot$ . We also set logarithmically flat distribution for a semi-major axis with a range of  $10R_\odot$  to  $10^6R_\odot$ . The initial eccentricity is supposed to be thermally distributed (Heggie 1975). As mentioned in subsection 2.1, we track the evolution of  $10^7$  initial binaries per each SN/kick model and a choice of  $\alpha$ . At the beginning of the binary evolution, both stars are in the ZAMS stage.

## 2.3. Tracking the Motion of BH-LC Binaries

For those that survive as BH-LC binaries in the present day, we calculate the motion of each binary in the Galaxy from BH formation to today. We follow the formulations of Tsuna et al. (2018), which numerically solved the orbits

of isolated BHs under the Galactic potential of [Irrgang et al. \(2013\)](#) (their Model II) that contains a spherical bulge, disc and spherical halo. The numerical code calculates the orbit using the cylindrical coordinates  $(R, \phi, z)$ , with a 4 th-order Runge-Kutta integration.

The displacement of the binary from its birth to BH formation is neglected, and we set the initial  $R$  and  $z$  coordinates to be those of the binary. Since both the binaries and the Galactic potential follow axisymmetric distributions, we randomize the initial azimuthal angle  $\phi$  from 0 to  $\pi/8$ . That enables us to increase the number of BH-LC binary samples effectively (see section 2.4). We define the initial velocity of the binary by adding the kick to the Galactic rotation velocity, approximated by a rotation curve of

$$v_\phi(r) = \begin{cases} 265 - 1875(r_{\text{kpc}} - 0.2)^2 & \text{km s}^{-1} & (\text{for } r_{\text{kpc}} < 0.2) \\ 225 + 15.625(r_{\text{kpc}} - 1.8)^2 & \text{km s}^{-1} & (\text{for } 0.2 < r_{\text{kpc}} < 1.8) \\ 225 + 3.75(r_{\text{kpc}} - 1.8) & \text{km s}^{-1} & (\text{for } 1.8 < r_{\text{kpc}} < 5.8) \\ 240 & \text{km s}^{-1} & (\text{for } r_{\text{kpc}} > 5.8), \end{cases} \quad (14)$$

where  $r_{\text{kpc}} \equiv r/(1 \text{ kpc})$ . For each binary we consider 10 randomized realizations of the kick orientation, assuming it follows an isotropic distribution. Figure 1 is an example of the Galactic path of a BH-LC binary in the  $x - y$  (*i.e.* the Galactic plane) and  $x - z$  planes. The star marker corresponds to the starting point of the binary at BH formation.

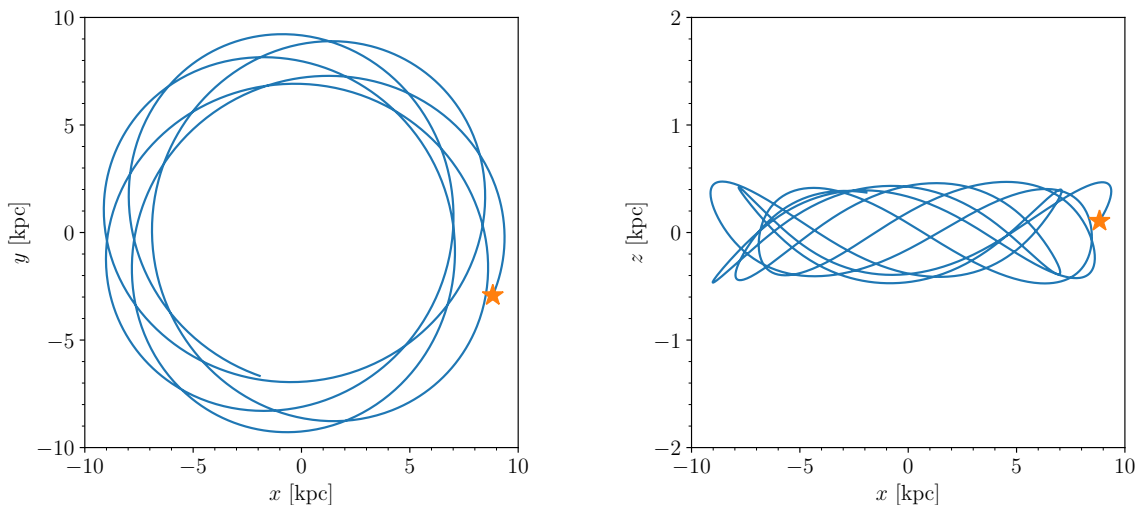


**Figure 1.** An example of the Galactic path of a BH-LC binary in  $x - y$  plane (the Galactic plane) and  $x - z$  one. The star markers show the initial location of the binary. The path is tracked for 1 Gyr from now (*i.e.*  $\tau = 0$ ).

#### 2.4. Effective Sampling Technique

In order to perform our simulation efficiently, we employ two sampling techniques in spatial and temporal ways. First, we utilize the fact that both the binary distribution and the Galactic potential adopted in our work are axisymmetric. The azimuthal angle distribution of initial binaries are limited to  $0 - \pi/8$ . After tracking the motions of them, we then move the azimuthal angle of the binaries by  $\pi/8$ , and repeat that for  $2\pi/(\pi/8) = 16$  times. The number of rotations is chosen so that the final number of detectable binaries sufficiently converge. This sampling technique enables us to increase the number of initial samples to  $16 \times 10^7$ .

Our previous work ([Shikauchi et al. 2022](#)) found that massive stars with short lifetimes significantly contribute to the luminous sources detectable with *Gaia*, owing to their much larger luminosity. We thus take an importance sampling

approach<sup>2</sup> by employing a bias factor  $b(\tau)$ ,

$$b(\tau) = \begin{cases} N \times f \times n_{\text{young}} \exp\left(-\frac{\tau_m - \tau}{\tau_{\text{SFR}}}\right) & \text{(the thin disc, } 0 \text{ Gyr} < \tau < 0.1 \text{ Gyr)}, \\ N \times (1 - f) \times \frac{M_{\text{disc}}/2}{M_{\text{tot}}} \times n_{\text{older}} \exp\left(-\frac{\tau_m - \tau}{\tau_{\text{SFR}}}\right) & \text{(the thin disc, } 0.1 \text{ Gyr} < \tau < 8 \text{ Gyr)}, \\ N \times (1 - f) \times \frac{M_{\text{disc}}/2}{M_{\text{tot}}} \times n_{\text{thick}} \exp\left(-\frac{\tau_m - \tau}{\tau_{\text{SFR}}}\right) & \text{(the thick disc, } 8 \text{ Gyr} < \tau < 12 \text{ Gyr)}, \\ N \times (1 - f) \times \frac{M_{\text{bulge}}}{M_{\text{tot}}} \times \beta(2, 3)(\tau) & \text{(the bulge, } 6 \text{ Gyr} < \tau < 12 \text{ Gyr)}. \end{cases} \quad (15)$$

where

$$\begin{cases} n_{\text{young}} = \frac{1}{\int_{\tau=0}^{0.1 \text{ Gyr}} \exp\left(-\frac{\tau_m - \tau}{\tau_{\text{SFR}}}\right) d\tau}, \\ n_{\text{older}} = \frac{1}{\int_{\tau=0.1 \text{ Gyr}}^{8 \text{ Gyr}} \exp\left(-\frac{\tau_m - \tau}{\tau_{\text{SFR}}}\right) d\tau}, \end{cases} \quad (16)$$

and  $f$  is a weight factor, 0.5. This biased function  $b(\tau)$  shows that 50 % of the total initial binaries with lookback time restricted to  $\tau < 0.1$  Gyr, and the rest is assigned to thin disc with  $\tau > 0.1$  Gyr, thick disc, and the bulge component. After simulating binary evolution, by multiplying a “weighting factor”  $w(\tau)$ ,

$$w(\tau) = \frac{p(\tau)}{b(\tau)} = \begin{cases} \frac{\frac{M_{\text{disc}}}{2M_{\text{tot}}} n_{\text{thin}}}{f n_{\text{young}}} & \text{(the thin disc, } 0 \text{ Gyr} < \tau < 0.1 \text{ Gyr)}, \\ \frac{n_{\text{thin}}}{(1-f)n_{\text{older}}} & \text{(the thin disc, } 0.1 \text{ Gyr} < \tau < 8 \text{ Gyr)}, \\ \frac{1}{1-f} & \text{(the thick disc)}, \\ \frac{1}{1-f} & \text{(the bulge)}, \end{cases} \quad (17)$$

to the BH-LC binary population, we obtain the unbiased population while at the same time having the bright LCs with short lifetimes sufficiently sampled.

### 2.5. The Detection Criteria

After obtaining the present-day location of BH-LC binaries, we calculate their detectability with *Gaia* by imposing the detection criteria of Yamaguchi et al. (2018) and Shikauchi et al. (2022)<sup>3</sup>.

We employ three constraints and obtain the maximum distance  $D_{\text{max}}$  within which each BH binary can be detected. If the distance to the BH binary  $D$  is smaller than  $D_{\text{max}}$ , we regard them as detectable.

#### 2.5.1. Limitation from Interstellar Extinction

The first restriction is that the apparent magnitude of a LC  $m_V(L_{\text{LC}}, T_{\text{eff,LC}}, D_{\text{LC}}, z_{\text{LC}})$  should be smaller than *Gaia*’s limiting magnitude in G band  $m_{V,\text{lim}} = 20$  (Gaia Collaboration et al. 2016), that is,

$$m_V(L_{\text{LC}}, T_{\text{eff,LC}}, D_{\text{LC}}, z_{\text{LC}}) = m_{V,\text{lim}}, \quad (19)$$

where  $L_{\text{LC}}$  is the LC luminosity,  $T_{\text{eff,LC}}$  is the effective temperature of a LC,  $D_{\text{LC}}$  is the maximum distance where the LC satisfies this condition and  $z_{\text{LC}}$  is the height of the LC from the Galactic plane.

The absolute magnitude of a LC  $M_V(L_{\text{LC}}, T_{\text{eff,LC}})$  can be obtained from  $L_{\text{LC}}$  and  $T_{\text{eff,LC}}$  with a bolometric correction (*c.f.* equation 1, 10, and Table 1 in Torres 2010). Note that we substitute G band with V band. This is a valid approximation for stars bluer than G type stars whose color  $V - I$  is less than one and the color  $|V - G|$  is almost zero according to Figure 11 and 14 of Jordi et al. (2010). The apparent magnitude of a LC  $m_V$  is expressed as a function of the distance to BH binary  $D$  and the height from the Galactic plane to the binary  $z$ ,

$$m_V = M_V(L_{\text{LC}}, T_{\text{eff,LC}}) + 5(2 + \log_{10} D/\text{kpc}) + A_V(D, z), \quad (20)$$

<sup>2</sup> [https://en.wikipedia.org/wiki/Importance\\_sampling#Application\\_to\\_simulation](https://en.wikipedia.org/wiki/Importance_sampling#Application_to_simulation)

<sup>3</sup> Note that *Gaia* BH 1, the confirmed BH-LC binary in *Gaia* DR3 (El-Badry et al. 2023), is correctly flagged as detectable by our detection criteria.

where  $D/\text{kpc}$  is  $D$  in units of kpc. The term  $A_V$  due to interstellar extinction can be expressed following [Shafter \(2017\)](#),

$$A_V(D, z) = a_V \int_0^D e^{-|z|/h_z} dD' \quad (21)$$

$$= a_V \frac{D h_z}{|z|} \left[ 1 - \exp\left(-\frac{|z|}{h_z}\right) \right], \quad (22)$$

where  $a_V$  is the average extinction rate in the Galactic plane ( $z = 0$ ), 1 mag/kpc, and  $h_z = 100$  pc is the scale height in the  $z$ -direction perpendicular to the plane ([Spitzer 1978](#)). Thus, the maximum distance satisfying the condition  $D_{\text{LC}}$  is

$$M_V(L_{\text{LC}}, T_{\text{eff,LC}}) + 5(2 + \log_{10} D_{\text{LC}}/\text{kpc}) + A_V(D_{\text{LC}}, z_{\text{LC}}) = m_{V,\text{lim}}. \quad (23)$$

Note that  $D_{\text{LC}}$  depends on the line-of-sight angle with respect to the plane, since the extinction term  $A_V$  depends on  $z_{\text{LC}}$ .

### 2.5.2. Constraints for Confirmed Detection of BHs

In astrometric observations, we can only identify BHs or NSs based on their masses. In order to consider unseen objects as BHs, we restrict the minimum mass of them to be measured as larger than  $2M_{\odot}$ ,

$$m_{\text{unseen}} - n\sigma_{\text{unseen}} > 2M_{\odot}, \quad (24)$$

where  $m_{\text{unseen}}$  is their true mass and  $\sigma_{\text{unseen}}$  is its standard error. We follow [Yamaguchi et al. \(2018\)](#) and adopt  $n = 1$ . Though the minimum limit we set here may induce contamination of NSs, searching for compact objects with masses of  $2 - 3M_{\odot}$  should be valuable as the existence of such an object was reported in gravitational wave searches (GW190814, [Abbott et al. 2020](#)).

From Kepler's third law the binary parameters, LC mass  $m_{\text{LC}}$ , BH mass  $m_{\text{BH}}$ , orbital period  $P$  and semi-major axis  $a$ , are correlated. Considering that  $a$  can be expressed by a multiplication of an angular semi-major axis  $a^*$  and the distance to BH-LC binary  $D$ , the correlation of binary parameters is shown as

$$\frac{(m_{\text{LC}} + m_{\text{BH}})^2}{m_{\text{BH}}^3} = \frac{G}{4\pi^2} \frac{P^2}{(a^* D)^3}, \quad (25)$$

where  $G$  is the gravitational constant. Ignoring the correlation of each parameter and observational errors, we derive a relationship between each parameter and its standard error,

$$\left(\frac{\sigma_{\text{BH}}}{m_{\text{BH}}}\right)^2 = \left(\frac{3}{2} - \frac{m_{\text{BH}}}{m_{\text{BH}} + m_{\text{LC}}}\right)^{-2} \left[ \left(\frac{m_{\text{LC}}}{m_{\text{BH}} + m_{\text{LC}}}\right)^2 \frac{\sigma_{\text{LC}}^2}{m_{\text{LC}}^2} + \frac{\sigma_P^2}{P^2} + \frac{9}{4} \left(\frac{\sigma_{a^*}^2}{a_*^2} + \frac{\sigma_D^2}{D^2}\right) \right]. \quad (26)$$

where  $\sigma$  is a standard error and each suffix corresponds to each binary parameter.

For confident detection of BHs, we impose a condition that the error of each parameter must be smaller than 10 % of the true value,

$$\frac{\sigma_{\text{LC}}}{m_{\text{LC}}} < 0.1, \frac{\sigma_P}{P} < 0.1, \frac{\sigma_{a^*}}{a_*} < 0.1, \text{ and } \frac{\sigma_D}{D} < 0.1. \quad (27)$$

Under these requirements, detection of BHs with  $m_{\text{BH}} \gtrsim 3.4M_{\odot}$  should be confirmed as BHs.

The conditions for LC mass and orbital period are easily satisfied. According to [Tetzlaff et al. \(2011\)](#), a standard error of LC mass based on its spectrum and luminosity is typically smaller than 10 %. Furthermore, the standard error of orbital periods is suppressed to below 10 % if the observed periods are shorter than 2/3 of the operation time of *Gaia* ([Esa 1997](#)). As [Lucy \(2014\)](#) and [O'Neil et al. \(2019\)](#) proposed a novel technique to estimate binary parameters when the orbital coverage is less than 40 %, and *Gaia* has been observing for more than five years, we employ 10 years as the maximum period of observable BH-LC binaries. For the lower limit of orbital periods, we set 50 days as [Yamaguchi et al. \(2018\)](#) does. The rest of the conditions in equation (27) impose two more constraints on  $D_{\text{max}}$ . First, considering that the parallax  $\Pi$  is proportional to the reciprocal of  $D$ , the ratio of the standard error of parallax  $\sigma_{\Pi}$  and  $\Pi$  can be approximated to that of  $\sigma_D$  and  $D$ ,

$$\frac{\sigma_{\Pi}}{\Pi} \sim \frac{\sigma_D}{D} < 0.1. \quad (28)$$

Gaia Collaboration et al. (2016) provided  $\sigma_{\Pi}$  in G band as a function of the apparent magnitude of a LC  $m_v$  and we employ the expression below ignoring the dependence on the color  $V - I$ ,

$$\sigma_{\Pi} = (-1.631 + 680.8z(m_v) + 32.73z(m_v)^2)^{1/2}[\mu\text{as}], \quad (29)$$

where

$$z(m_v) = 10^{0.4(\max[12.09, m_v] - 15)}. \quad (30)$$

Combining equations (28) and (29), the second constraint for  $D_{\max}$  is

$$\left(\frac{D_{\max}}{\text{kpc}}\right) < D_{\Pi} = \frac{10^2}{(-1.631 + 680.8z(m_v) + 32.73z(m_v)^2)^{1/2}}. \quad (31)$$

Finally, for the condition of angular semi-major axis, we approximate the uncertainty of the angular semi-major axis of a BH binary  $\sigma_{a^*}$  as that of its orbital radius on the celestial sphere  $\sigma_{\Pi}$ . Then, the final condition for  $D_{\max}$  can be obtained,

$$\left(\frac{D_{\max}}{\text{kpc}}\right) < D_a = \frac{am_{\text{BH}}}{10(m_{\text{BH}} + m_{\text{LC}})\sigma_{\Pi}}. \quad (32)$$

In summary, we obtain three constraints for  $D_{\max}$ ,  $D_{\text{LC}}$  (equation 23)  $D_{\Pi}$  (equation 31), and  $D_a$  (equation 32). For each BH binary sample, we compare the minimum of the three to the current distance to determine whether the binary is detectable.

### 3. RESULT

Based on the results of BSE and the orbit calculations, we obtain the spatial distributions and binary parameters of the Galactic BH-LC binaries. We summarize in Table 1 the number of BH-LC binaries in the MW with orbital periods of 50 days to 10 years and the detectability, for each SN/kick model and a choice of  $\alpha$ . The number of detectable binaries for each model is several times larger than estimated in our previous work (Shikauchi et al. 2022), which can be explained by the following differences between the two works. In this work, we have considered a realistic star formation history instead of a constant star formation rate. That drastically increases the number of BH binaries with low mass LCs ( $m_{\text{LC}} \lesssim 1M_{\odot}$ ), and also shows different BH/LC mass distributions from our previous work. Binary and spatial parameter distributions are shown in Appendix A. We have also employed a radial distribution with the number density proportional to  $R \exp(-R)$ , while the previous work adopted the distribution proportional to  $\exp(-R)$ . This effectively enhances the number of sources closer to us. Furthermore, while the previous work employed a single metallicity value of solar for all binaries, here we have considered the metallicity to vary as a function of radius and lookback time. As for binaries born in the past with generally lower metallicity, progenitors with smaller ZAMS masses can evolve into BHs instead of NSs due to reduced mass loss. In addition, the number of heavier BHs will increase, which would make the binary easier to detect.

SN model	kick	$\alpha$	$N_{\text{BH-LC, MW}}$	$N_{\text{det}}$	Shikauchi et al. (2022)
delayed	FB kick	1	$3.83 \times 10^3$	$7.22^{+5.98}_{-5.50}$	1.1
...	no kick	...	$1.04 \times 10^4$	$51.9^{+5.52}_{-10.9}$	22
rapid	FB kick	...	$9.14 \times 10^3$	$60.7^{+11.6}_{-6.03}$	18
delayed	FB kick	10	$7.68 \times 10^3$	$14.6^{+10.9}_{-0.19}$	9.4
...	no kick	...	$3.53 \times 10^4$	$67.4^{+11.4}_{-7.21}$	46
rapid	FB kick	...	$1.43 \times 10^4$	$92.0^{+6.79}_{-6.67}$	31

**Table 1.** The number of BH-LC binaries in the MW  $N_{\text{BH-LC, MW}}$  with  $P$  between 50 days and 10 years, and those detectable with *Gaia*  $N_{\text{det}}$ , for different choices of SN/kick models and values of the CE efficiency  $\alpha$ . The numbers and errors in  $N_{\text{det}}$  correspond to the median and the spread between 10 th and 90 th percentiles for the 10 realizations of the kick orientation.

In order to evaluate the correlation between each binary parameter and spatial parameters, we calculate the “weighted” Pearson correlation coefficients,

$$\rho_{XY, w} = \frac{\text{cov}(X, Y, w)}{\sqrt{\sigma_{X, w} \sigma_{Y, w}}}, \quad (33)$$

where  $X, Y$  are choices of binary parameters and spatial information,  $\text{cov}(X, Y, w)$  is a weighted covariance matrix of  $X$  and  $Y$ ,

$$\text{cov}(X, Y, w) = \frac{\sum_i (w_i \times (X_i - \bar{X}) \times (Y_i - \bar{Y}))}{\sum_i w_i}, \quad (34)$$

$w$  is the weighting factor for each binary (see equation 18),  $\bar{X}, \bar{Y}$  are weighted means of  $X$  and  $Y$ , and  $\sigma_{X,w}, \sigma_{Y,w}$  are weighted standard deviations of  $X, Y$ , *i.e.*  $\text{cov}(X, X, w)$  and  $\text{cov}(Y, Y, w)$ .

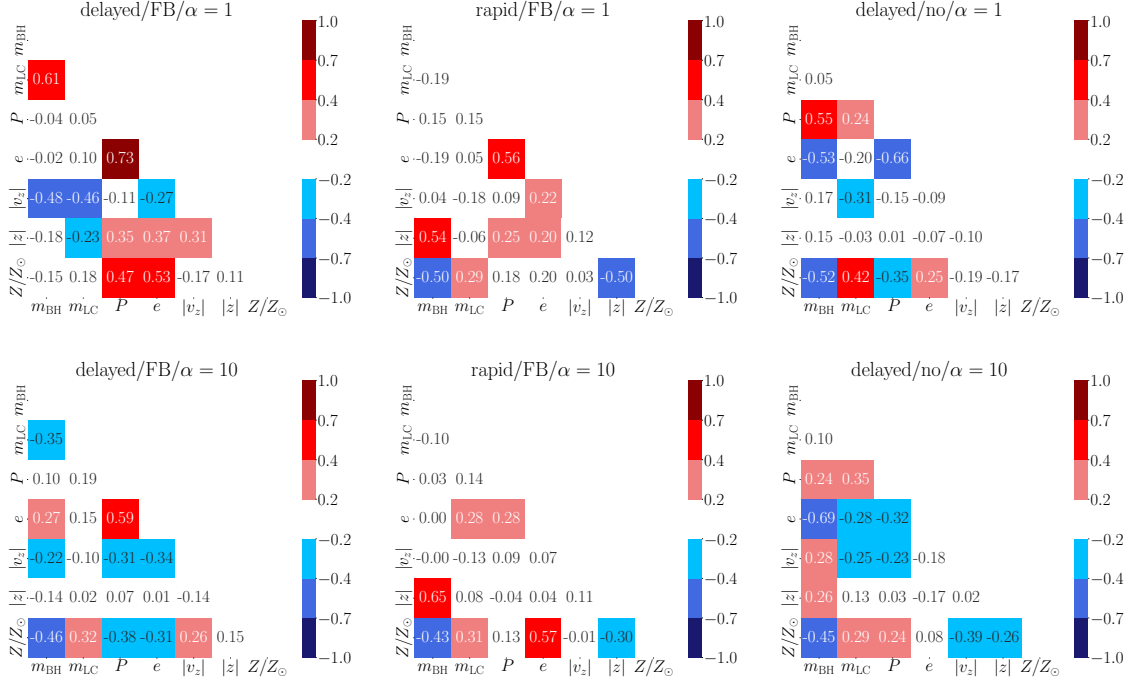


**Figure 2.** Correlation coefficients between the current binary parameters (BH mass  $m_{\text{BH}}$ , LC mass  $m_{\text{LC}}$ , orbital periods  $P$ , and eccentricities  $e$ ), the current spatial parameters (velocities perpendicular to the Galactic plane  $|v_z|$  and the heights from the Galactic plane  $|z|$ ), and metallicity  $Z/Z_{\odot}$  of the detectable BH-LC binaries, for different choices of the SN/kick models and values of the CE efficiency  $\alpha$ .

The coefficients of the detectable BH-LC binaries with each SN/kick model and value of the CE efficiency  $\alpha$  are summarized in Figure 2. Values of the coefficients are categorized to seven levels: “strongly positive correlation” ( $1.0 \sim 0.7$ ), “positive correlation” ( $0.7 \sim 0.4$ ), “weakly positive correlation” ( $0.4 \sim 0.2$ ), “no correlation” ( $0.2 \sim -0.2$ ), “weakly negative correlation” ( $-0.2 \sim -0.4$ ), “negative correlation” ( $-0.4 \sim -0.7$ ), and “strongly negative correlation” ( $-0.7 \sim -1$ ). Figure 3 shows correlation coefficients for the entire Galactic binary population with orbital periods from 50 days to 10 years, for each SN/kick model and  $\alpha$ . Most of them show no correlations. Correlation coefficients seen in the detectable BH-LC binaries have the opposite sign and/or are enhanced compared with the correlations among the Galactic BH-LC population. Thus, most of the correlations are generally biased by the detection criteria.

Here, we look into significant correlations of the detectable BH-LC binaries in each model. In the delayed SN model with FB kick and  $\alpha = 1$ ,

1. strongly positive correlation of  $(P, e)$ ,
2. positive correlations of  $(m_{\text{BH}}, m_{\text{LC}})$ ,  $(P, Z/Z_{\odot})$ , and  $(e, Z/Z_{\odot})$ ,
3. negative correlations of  $(m_{\text{BH}}, |v_z|)$  and  $(m_{\text{LC}}, |v_z|)$ ,

are seen. The strongly positive correlation can be understood based on the positive correlations of  $(P, Z/Z_{\odot})$ ,  $(e, Z/Z_{\odot})$ . Heavier BH binaries are formed in lower metallicity, suffering from smaller fallback kick. This results in less eccentric

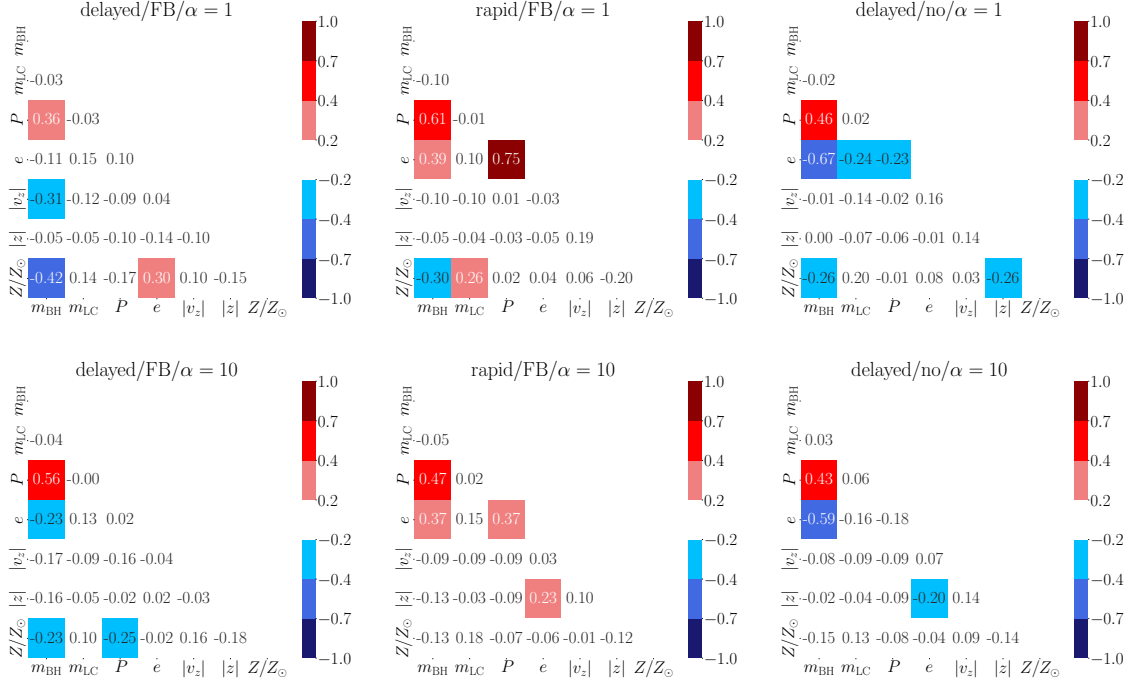


**Figure 3.** Same as Figure 2, but for the entire Galactic BH-LC binary population with orbital periods from 50 days to 10 years.

and narrower orbits compared to binaries with lighter BHs. The positive correlation of  $(m_{\text{BH}}, m_{\text{LC}})$  is highlighted by the detection criteria. Heavier BHs can swing around heavier LCs largely and are more detectable.

The negative correlation of  $(m_{\text{BH}}, |v_z|)$  is easily understandable, considering that lighter BHs suffer from larger FB kick. This trend matches the observations of the Galactic XRBs (Gandhi et al. 2019). The negative correlation of  $(m_{\text{LC}}, |v_z|)$  can be interpreted as peculiar motion of the binary is proportional to  $m_{\text{BH}}/(m_{\text{BH}} + m_{\text{LC}})$ .

In the rapid SN model with FB kick and  $\alpha = 1$ ,

1. positive correlations of  $(m_{\text{BH}}, |z|)$  and  $(P, e)$ ,
2. negative correlations of  $(m_{\text{BH}}, Z/Z_{\odot})$  and  $(|z|, Z/Z_{\odot})$

are seen. The positive correlation of  $(P, e)$  exists as well, but can be interpreted in a different way from in the delayed SN model with FB kick. In the rapid SN model, natal kick is not as strong as in the delayed SN model. Thus, BH binaries experiencing the CE phase simply have smaller eccentricities and narrower orbits.

The weaker natal kick in the rapid model also explains the positive correlation of  $(m_{\text{BH}}, |z|)$ . In the delayed SN model with FB kick, lighter BH binaries can move farther away from the Galactic plane due to strong FB kick. However, such light BHs are rarely formed in the rapid SN model and BH binaries do not go farther. Rather, the detection criteria highlight the fact that heavier BH binaries are detectable at farther distances according to equation 32.

The negative correlation of  $(m_{\text{BH}}, Z/Z_{\odot})$  is easily understood considering heavier BHs are formed in lower metallicities. The negative correlation of  $(|z|, Z/Z_{\odot})$  can be interpreted according to the correlations of  $(m_{\text{BH}}, Z/Z_{\odot})$ ,  $(m_{\text{BH}}, |z|)$ .

Comparing with the result in the delayed SN model with FB kick, the correlation coefficients of  $(m_{\text{BH}}, |z|)$  ( $-0.18$  with the delayed SN model,  $0.54$  with the rapid SN model) have the opposite signs. As mass gap BHs ( $m_{\text{BH}} \lesssim 5M_{\odot}$ ) will be detectable only in the delayed SN model, the distribution of  $(m_{\text{BH}}, |z|)$  would be a powerful tool to constrain the SN model.

In the delayed SN model with no kick and  $\alpha = 1$ , there are

1. positive correlations of  $(m_{\text{BH}}, P)$  and  $(m_{\text{LC}}, Z/Z_{\odot})$ ,
2. negative correlations of  $(m_{\text{BH}}, e)$ ,  $(m_{\text{BH}}, Z/Z_{\odot})$ , and  $(P, e)$ .

The positive correlation of  $(m_{\text{BH}}, P)$  can be interpreted as follows. For light BH binaries, BHs are formed after the CE phase. On the other hand, heavier BH binaries ( $m_{\text{BH}} \gtrsim 10M_{\odot}$ ) do not experience the CE phase because they cannot

survive if they enter the phase as shown below. Since heavy BHs are formed in low metallicity, heavy BH binaries are typically born in the distant past. They tend to have low mass LCs ( $m_{\text{LC}} \lesssim 1M_{\odot}$ ), otherwise they cannot exist as BH-LC binaries until the present day. However, the ZAMS masses of the progenitors of these heavy BHs are as large as  $\gtrsim$  tens of  $M_{\odot}$ . Here, we roughly estimate the final orbital separations if such high mass ratio binaries enter the CE phase. Considering  $\alpha\lambda$  prescription of the CE phase, the binding energy of a binary at the beginning of the CE phase is roughly proportional to the orbital energy of a binary at the end of the phase. Orbital separations at the final stage of the CE phase  $a_f$  can be approximated as

$$a_f = \frac{m_{\text{prim,core}}m_{\text{second,ZAMS}}}{2} \times \left( \frac{m_{\text{prim,i}}m_{\text{prim,env}}}{\alpha\lambda R} + \frac{m_{\text{prim,i}}m_{\text{second,ZAMS}}}{2a_i} \right)^{-1} \quad (35)$$

$$\sim \frac{\alpha\lambda}{2} \times \frac{m_{\text{second,ZAMS}}m_{\text{prim,core}}}{m_{\text{prim,i}}m_{\text{prim,env}}} R, \quad (36)$$

where we have defined the initial secondary mass  $m_{\text{second,ZAMS}}$ , the primary mass at the beginning of the CE phase  $m_{\text{prim,i}}$ , the envelope mass of the primary  $m_{\text{prim,env}}$ , the core mass of the primary  $m_{\text{prim,core}}$ , the orbital separation at the beginning of the phase  $a_i$  and Roche lobe radius of the primary  $R$ . Assuming that mass loss is negligible in low metallicity,  $m_{\text{prim,i}} \sim m_{\text{prim,ZAMS}}$  and  $m_{\text{prim,core}}/m_{\text{prim,env}} \sim 0.5$  is almost independent of the primary mass (*e.g.* section 4.2 in [Sukhbold et al. 2018](#)). Since  $R$  is approximated to tens of solar radii and  $\lambda \sim 0.4$ ,  $a_f \lesssim 0.1R_{\odot}$  with  $\alpha = 1$ , and  $\lesssim R_{\odot}$  even for  $\alpha = 10$ . It is smaller than the core radius of the primary,  $\sim R_{\odot}$ , which leads high mass ratio binaries with  $m_{\text{second,ZAMS}}/m_{\text{prim,ZAMS}} \ll 1$  to merge. Thus, existing binaries with heavy BHs are limited to have longer orbital periods that do not experience the CE phase.

The positive correlation of  $(m_{\text{LC}}, Z/Z_{\odot})$  is easily explained by the fact that only massive LCs that were born recently can survive until today. The negative correlations of  $(m_{\text{BH}}, e)$  is understandable as lighter BH binaries suffer from larger Blaauw kicks. Combining correlations of  $(m_{\text{BH}}, P)$  and  $(m_{\text{BH}}, e)$ , the negative correlation of  $(P, e)$  would be reasonable.

Comparing the correlation coefficients in the delayed SN model with/without FB kick, a correlation of  $(P, e)$  (0.73 with FB kick model,  $-0.66$  without FB kick) are significant and have the opposite trend. Correlations of  $(m_{\text{BH}}, |z|)$  ( $-0.18$  with FB kick,  $0.15$  without FB kick) might be a clue for the strength of natal kick as well, although they are less significant. Due to the absence of FB kick, binaries with light BHs do not have as large kick or move as far as the model including FB kick. The detection criteria highlight that heavier BH binaries can be detected farther away, which might result in very weakly positive correlations of  $(m_{\text{BH}}, |z|)$ . Thus, we expect that we would give a constraint on the strength of natal kicks by checking these correlations from the observed BH-LC samples.

In the delayed SN model with FB kick and  $\alpha = 10$ ,

1. a positive correlation of  $(P, e)$ ,
2. a negative correlation of  $(m_{\text{BH}}, Z/Z_{\odot})$

exist. Correlations of  $(P, e)$ ,  $(m_{\text{BH}}, Z/Z_{\odot})$  are still seen in the higher CE efficiency case. A correlation of  $(m_{\text{BH}}, |z|)$  is somewhat blurred, but still exists. That might be because most of the light BH binaries seen in  $\alpha = 1$  will be disrupted during BH formation. Considering they experience the CE phase, the orbits after the phase will be wider for higherr  $\alpha$ , hence easier to disrupt. Correlations of  $(P, e)$ ,  $(m_{\text{BH}}, |z|)$  could be a clue for the strength of natal kick and SN model, regardless of the CE efficiency.

With the high CE efficiency in the rapid SN model, we see

1. positive correlations of  $(m_{\text{BH}}, |z|)$  and  $(e, Z/Z_{\odot})$ ,
2. a negative correlation of  $(m_{\text{BH}}, Z/Z_{\odot})$ .

All the significant correlations follow or enhance the trend in  $\alpha = 1$  case. As correlations of  $(m_{\text{BH}}, |z|)$  retains the same trend in  $\alpha = 1$  case, they would be useful to constraint SN model even if the CE efficiency is high.

Finally, in the delayed SN model without FB kick and  $\alpha = 10$ ,

- negative correlations of  $(m_{\text{BH}}, e)$  and  $(m_{\text{BH}}, Z/Z_{\odot})$

are seen. They follow the trend seen in  $\alpha = 1$  case. The correlations  $(P, e)$ ,  $(m_{\text{BH}}, |z|)$  are somewhat blurred compared to the  $\alpha = 1$  case, but still exist. The trend of  $(P, e)$  could be explained as follows. Due to the high CE efficiency, lighter BH binaries can survive the CE phase and their final orbits can be as wide as heavy BH binaries seen in  $\alpha = 1$ . That blurs the correlation of  $(m_{\text{BH}}, P)$ , resulting in blurring the correlation of  $(P, e)$ . Also, the contribution of light BH binaries with larger orbital periods might explain the trend of  $(m_{\text{BH}}, |z|)$ . As a number of light BH binaries can have longer orbital periods, they are easier to detect compared to  $\alpha = 1$  case. That would weigh the distribution of  $(m_{\text{BH}}, |z|)$  to light BHs, resulting in blurring the correlation of  $(m_{\text{BH}}, |z|)$ . Nonetheless, correlations of  $(P, e)$ ,  $(m_{\text{BH}}, |z|)$  would give us a clue for the strength of FB kick in the high CE efficiency case.

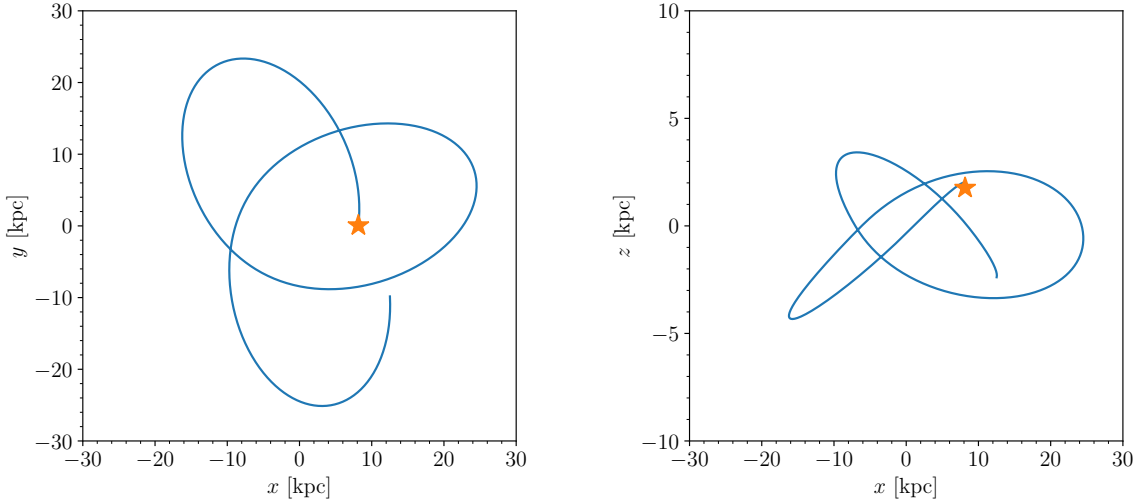


**Figure 4.** The same as Figure 1, but for a binary traveling the MW with an eccentric orbit of  $e_{\text{gal}} \sim 0.5$  (see main text for the definition of  $e_{\text{gal}}$ ).

In summary, correlations of

- $(m_{\text{BH}}, |z|)$  ( $-0.18$  in the delayed SN model,  $0.54$  in the rapid SN model with FB kick and  $\alpha = 1$ )

have the opposite signs by the choice of SN model. Considering mass gap BHs can be detected only in the delayed SN model, the distribution of  $(m_{\text{BH}}, |z|)$  might provide an important clue to constrain the SN model.

Correlations of

1.  $(P, e)$  ( $0.73$  and  $-0.66$  for delayed SN model with and without FB kick for  $\alpha = 1$  case respectively),
2.  $(m_{\text{BH}}, |z|)$  ( $-0.18$  with FB kick,  $0.15$  without FB kick in  $\alpha = 1$ )

have the opposite signs depending on the existence of FB kick. Thus these correlations would give a constraint on the strength of natal kick. All of the trends summarized above would be preserved even if the CE efficiency is high.

Finally, we investigated how eccentric are the motions of BH-LC binaries in the Galactic potential. A characteristic quantity we defined is “galactic eccentricity”  $e_{\text{gal}}$ . It is defined by the maximum and the minimum radius  $r_{\text{max}}, r_{\text{min}}$  at which each binary have reached during its lifetime,  $e_{\text{gal}} \equiv (r_{\text{max}} - r_{\text{min}})/(r_{\text{max}} + r_{\text{min}})$ . For all the SN/kick models with  $\alpha = 1$ , almost all ( $\gtrsim 99\%$ ) of the binaries have almost circular ( $e_{\text{gal}} < 0.1$ ) motion in the Galactic potential like shown in Figure 1. In the SN models with FB kick,  $0.5\%$  (delayed) and  $0.1\%$  (rapid) binaries have eccentric orbits with  $e_{\text{gal}} > 0.5$ . An example of the Galactic path for one of the binaries is shown in Figure 4.

#### 4. COMPARISON WITH THE CONFIRMED BH BINARY AND THE BH CANDIDATES WITH *GAIA*

In this section, we compare our results with BH candidates reported in *Gaia* DR3. First, we review the candidates found in spectroscopic or astrometric data. Then, we select some candidates among them and discuss how they can be formed from isolated field binaries.

From the data of single-lined spectroscopic binaries, the *Gaia* collaboration reported possible candidates of binaries consisting of compact objects with MS or post-MS stars (Gaia Collaboration et al. 2022). However, El-Badry &

Rix (2022) immediately rejected the possibility of possessing BHs for all of the BH-MS star binary candidates by combining other spectroscopic data. Jayasinghe et al. (2022) selected 234 single-lined binaries and investigated the possibility of BHs, resulting in rejecting the possibility for all the candidates. Though BH-MS star candidates in *Gaia* Collaboration et al. (2022) have been rejected, BH-post MS star candidates reported in *Gaia* Collaboration et al. (2022) and ellipsoidal variables (Gomel et al. 2022) still remain. For BH-post MS star binaries it is difficult to estimate the masses of post-MS stars. Thus we can only obtain lower limits of the masses of the unseen objects, which makes us hard to identify BH-post MS star binary candidates. Follow-up observations with spectroscopy in other wavelengths will provide details on the light curves of LCs and then reveal the nature of them by fitting models to the spectra as El-Badry & Rix (2022) did.

Also, some researches found BH-LC binary candidates from *Gaia* DR3 data. Andrews et al. (2022) found 24 candidates possibly including BHs or NSs, with long orbital period such as  $\sim$ years from astrometric binaries. Shahaf et al. (2022) applied their own triage technique (Shahaf et al. 2019) for astrometric data, and found eight candidates including massive unseen objects heavier than  $2.4M_{\odot}$ . Tanikawa et al. (2022) reported the existence of a BH-LC binary candidate, with the longest orbital period among the reported BH candidates so far. El-Badry et al. (2023) confirmed *Gaia* DR3 4373465352415301632 (hereafter *Gaia* BH 1), a binary with a BH of  $m_{\text{BH}} = 9.78 \pm 0.18M_{\odot}$  and a G dwarf star  $m_{\text{LC}} = 0.93 \pm 0.05M_{\odot}$  with orbital period  $P = 185.63 \pm 0.05$  days and a modest eccentricity  $e \sim 0.45$ . This binary is located at 480 pc from the Earth, and is identified as the nearest BH currently observed. Chakrabarti et al. (2022) rejected any possibilities of luminous stars for the unseen object, and confirmed *Gaia* BH 1 as a BH-MS star binary as well.

Including *Gaia* BH 1, we select the candidates with the upper limit of compact object mass larger than  $3M_{\odot}$  from Andrews et al. (2022); Shahaf et al. (2022); Tanikawa et al. (2022) since BSE considers compact objects heavier than  $3M_{\odot}$  as BHs. These BH candidates can be roughly divided into two types in terms of component mass and orbital period: one is  $\lesssim 4M_{\odot}$  BH and  $\lesssim 1.5M_{\odot}$  LC binaries with long orbital periods ( $P \sim 1.5 - 4$  years) and non-zero eccentricities (type 1) and the other is  $\gtrsim 9M_{\odot}$  BH and  $\lesssim 1.2M_{\odot}$  LC binaries with short orbital periods ( $P \lesssim 1$  year) and non-zero eccentricities (type 2). The latter type includes *Gaia* BH 1. We summarize the BH candidates and *Gaia* BH 1 in Table 2. We note that the LC mass of the candidate reported in Tanikawa et al. (2022) is not estimated, so we do not categorize it as either type.

<i>Gaia</i> ID	BH mass [ $M_{\odot}$ ]	LC mass [ $M_{\odot}$ ]	$P$ [days]	$e$	type
4314242838679237120 <sup>*1</sup>	$2.25^{+1.87}_{-0.84}$	0.63 – 1.00	$1146 \pm 382$	$0.70 \pm 0.09$	1
5593444799901901696 <sup>*1</sup>	$2.57^{+0.86}_{-0.69}$	$1.27 \pm 0.2$	$1039 \pm 292$	$0.44 \pm 0.14$	1
6328149636482597888 <sup>*1</sup>	$2.71^{+1.50}_{-0.36}$	$1.21 \pm 0.2$	$736 \pm 23$	$0.14 \pm 0.07$	1
6281177228434199296 <sup>*2</sup>	$11.9 \pm 1.5$	1.0	$153.95 \pm 0.36$	$0.180 \pm 0.042$	2
3509370326763016704 <sup>*2</sup>	$3.69 \pm 0.24$	0.7	$109.392 \pm 0.065$	$0.237 \pm 0.016$	1
6802561484797464832 <sup>*2</sup>	$3.08 \pm 0.84$	1.2	$574.8 \pm 6.2$	$0.830 \pm 0.071$	1
3263804373319076480 <sup>*2</sup>	$2.75 \pm 0.50$	1.0	$510.7 \pm 4.7$	$0.278 \pm 0.023$	1
6601396177408279040 <sup>*2</sup>	$2.57 \pm 0.50$	1.0	$533.5 \pm 2.0$	$0.791 \pm 0.043$	1
4373465352415301632 <sup>*3</sup>	$9.78 \pm 0.18$	$0.93 \pm 0.05$	$185.63 \pm 0.05$	$0.454 \pm 0.005$	2
5870569352746779008 <sup>*4</sup>	$> 5.25$		$1352.25 \pm 45.50$	$0.5324 \pm 0.0095$	

**Table 2.** Information of the BH candidates reported in *Gaia* DR 3 whose BH mass exceeds  $3M_{\odot}$  at the upper limit and *Gaia* BH 1 (El-Badry et al. 2023). Binary parameters of the candidates are based on the *Gaia* DR3 database. We cited parameters estimated in El-Badry et al. (2023) for the information of *Gaia* BH 1.

\*1: reported in Andrews et al. (2022), \*2: reported in Shahaf et al. (2022), \*3: reported in El-Badry et al. (2023), and \*4: Tanikawa et al. (2022).

We found that the delayed SN model with no natal kick and  $\alpha = 10$  stably forms both types of BH binaries. Based on our simulation,  $\sim 3 \times 10^4$  type 1-like binaries and  $\sim 900$  type 2-like binary are expected to exist in the MW. Figure 5 shows examples of evolutionary path for both types of BH binaries in the delayed SN model with no kick and  $\alpha = 10$ . The evolutionary path for both types of binaries is almost the same: they experience the CE phase before forming BHs. The difference is that BH mass of type 1-like binaries is lighter. Thus, their mass loss kick (*i.e.* the Blaauw kick) is larger than that of type 2-like ones, which makes orbits of type 1-like binaries wider and more eccentric. The

delayed SN models with FB kick and  $\alpha = 10$  may also form both types of binaries. While type-1 like binaries are stably formed, type-2 like binaries were sometimes born if the strength of natal kick is relatively small such as tens of  $\text{km s}^{-1}$  to  $135 \text{ km s}^{-1}$ . The existence of natal kick can make the orbits of type 2-like binaries more eccentric ( $e \sim 0.3 - 0.6$ ) and narrower ( $P \sim 200$  days), more similar to *Gaia* BH 1.

However, the other models, *i.e.* the rapid SN model regardless of the CE efficiency or the delayed SN model with the low CE efficiency, cannot form both types of binaries. Light BH binaries with long orbital periods cannot be formed in the rapid SN model. Some BHs as light as  $\lesssim 4M_{\odot}$  are formed in the rapid SN model via accretion-induced collapse, but their orbital periods are shorter than 1 year. Thus, if we confirm that the candidates of type 1-like binaries possess BHs, SN models producing mass gap BHs like the delayed SN model is favored. In the delayed SN model with low CE efficiency, if one attempts to form Type 2-like binaries with heavier BHs, their final orbital periods become  $\sim 10$  days, much shorter than observed.

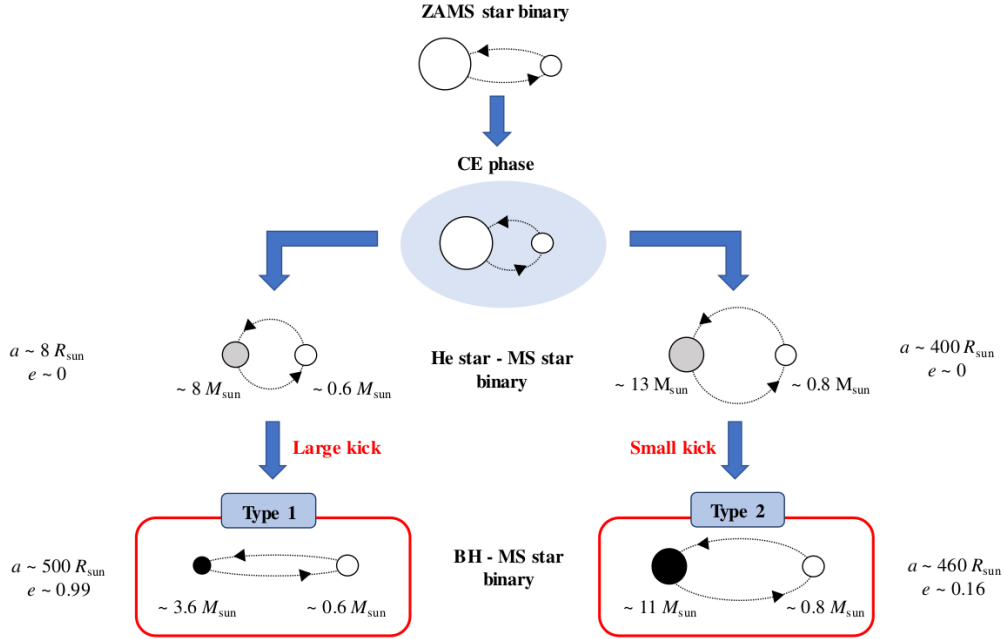


**Figure 5.** An example of evolutionary paths of type 1-like BH binary (*e.g.*  $\lesssim 4M_{\odot}$  BH and  $\lesssim 1.5M_{\odot}$  LC binaries with long orbital periods ( $P \sim 1.5 - 4$  years) and non-zero eccentricities) and type 2-like BH binary (*e.g.*  $\gtrsim 9M_{\odot}$  BH and  $\lesssim 1.2M_{\odot}$  LC binaries with short orbital periods ( $P \lesssim 1$  year) and non-zero eccentricities). Both types of binaries experience the CE phase and finally form different range of BH mass, which makes a difference in terms of orbital separations and eccentricities depending on the strength of mass loss kick.

## 5. CONCLUSION

We investigated correlations between binary parameters (BH mass, LC mass, orbital periods, and eccentricities), spatial parameters (velocities perpendicular to the Galactic plane, and the heights from the Galactic plane), and metallicity of BH-LC binaries detectable with *Gaia*. By sampling initial spatial conditions, metallicity and lookback time distributions based on Wagg et al. (2021), then simulating binary evolution with BSE and the orbit of the binary under the Galactic potential, we obtained the BH-LC binary population in the MW.

We conclude that most of the correlation coefficients among the detectable binaries have the opposite sign and/or are enhanced by the detection criteria as correlation coefficients among the Galactic population show almost no correlations. Nevertheless, we indicated some correlations might probe the SN model and the strength of natal kick regardless of the CE efficiency. Correlations of  $(m_{\text{BH}}, |z|)$  would be a clue for the SN model if a strong natal kick like FB kick exists. In the delayed SN model light BHs ( $m_{\text{BH}} \lesssim 4M_{\odot}$ ) are formed, and binaries possessing such BHs go farther from the Galactic plane due to strong kick, resulting in a negative correlation. On the other hand, in the rapid SN model, light BHs are rarely formed and natal kick is not so strong, thus BH binaries do not leave far away from the Galactic plane. The detection criteria simply emphasizes heavier BH binaries can be detected at farther distances.

The signs of correlations of  $(P, e)$ ,  $(m_{\text{BH}}, |z|)$  vary depending on the existence of FB kick, which would be useful to constraint the strength of natal kick. With FB kick, light BH binaries suffer from a strong kick, which makes their orbits more eccentric and wider. On the other hand, due to the absence of FB kick, light BH binaries can remain tighter than those in the same SN model with FB kick, resulting in a positive correlation of  $(m_{\text{BH}}, P)$  and the opposite correlation of  $(P, e)$ . The trend of  $(m_{\text{BH}}, |z|)$  might be understandable based on the similar reason discussed in the rapid SN model, *i.e.* light BH binaries cannot leave farther from the Galactic plane than those with FB kick and heavier BH binaries can be detected at farther distances.

Using BH-LC samples we employed here, we also investigated the possibility of forming binaries like the BH candidates reported in *Gaia* DR3 (Andrews et al. 2022; Shahaf et al. 2022) and *Gaia* BH 1 (El-Badry et al. 2023) in each SN/kick model with a choice of  $\alpha$  used in this work. We divided all the candidates and *Gaia* BH 1 into two groups, type 1 and 2 (see Table 2), in terms of component masses and orbital periods. We revealed that only the delayed SN model with the high CE efficiency can form both types of binaries in an isolated field. Both types of binaries are formed via the CE phase. If the CE efficiency is as low as unity, type 2-like binaries can not have as large orbital separations as the observed ones. Especially, the rapid SN model cannot form type 1-like binaries since such light BHs are formed via accretion-induced collapse, which requires shorter orbital separations than seen in type 1-like binaries. We also expect the SN model producing light BHs of masses  $\lesssim 4M_{\odot}$  would be favored if BH candidates categorized as type 1 binaries are confirmed as genuine BH binaries.

As more candidates are identified as genuine BH binaries, spatial distributions of BH-LC binaries in the Galactic coordinate will be obtained as shown in Figure 6. Each point in the figure depicts the detectable BH-LC binaries obtained from all the realizations, weighted by the weighting factor and colored by BH mass. In the delayed SN model, light BHs ( $m_{\text{BH}} \lesssim 5M_{\odot}$ ) would be detectable at a high longitude such as  $|b| > 45^{\circ}$ . Also, we expect  $|v_z|$  distributions might tell us the strength of natal kick. Figure 7 shows a probability density function of  $\log |v_z|$  of the detectable BH-LC binaries. If a strong natal kick model such as FB kick is favored,  $\gtrsim 50\%$  of the BH-LC binaries would have a large  $|v_z|$  such as  $\sim 30 \text{ km s}^{-1}$ . If SN model which does not produce lower mass gap BHs is favored, the detected BH-LC binaries are less likely to have such a large  $|v_z|$ .

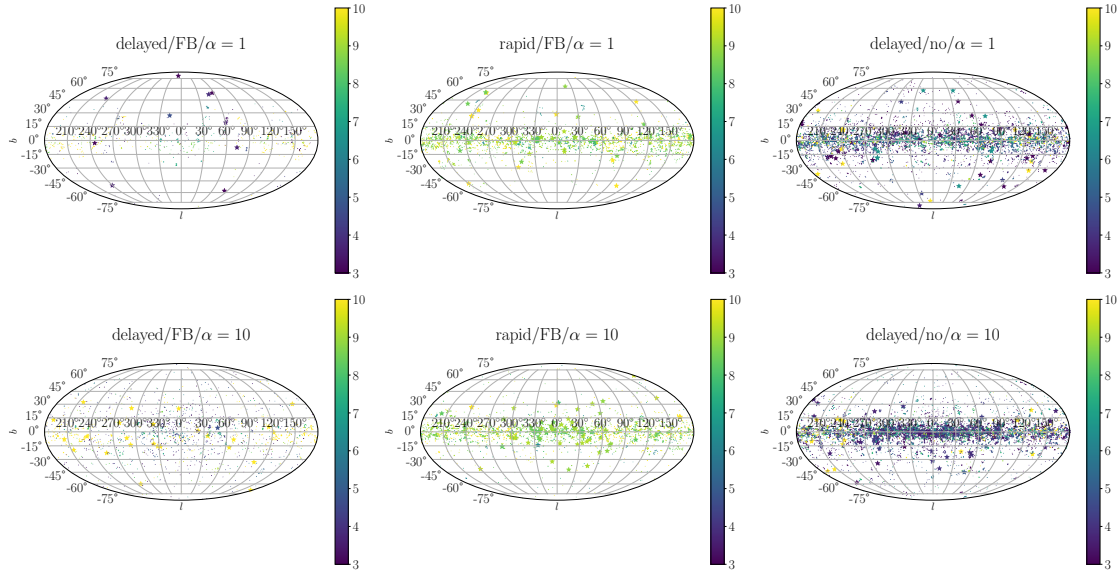


**Figure 6.** Spatial distributions of the detectable BH-LC binaries obtained from 10 different realizations with different choices of the SN/kick models and values of the CE efficiency  $\alpha$ . Maps are shown in the Galactic coordinate. Each star marker shows each binary, whose size is proportional to the weighting factor. Colors of each marker correspond to BH mass.

#### ACKNOWLEDGEMENT

M.S. is supported by Research Fellowships of Japan Society for the Promotion of Science for Young Scientists, by Forefront Physics and Mathematics Program to Drive Transformation (FoPM), a World-leading Innovative Graduate Study (WINGS) Program, the University of Tokyo, and by JSPS Overseas Challenge Program for Young Researchers.

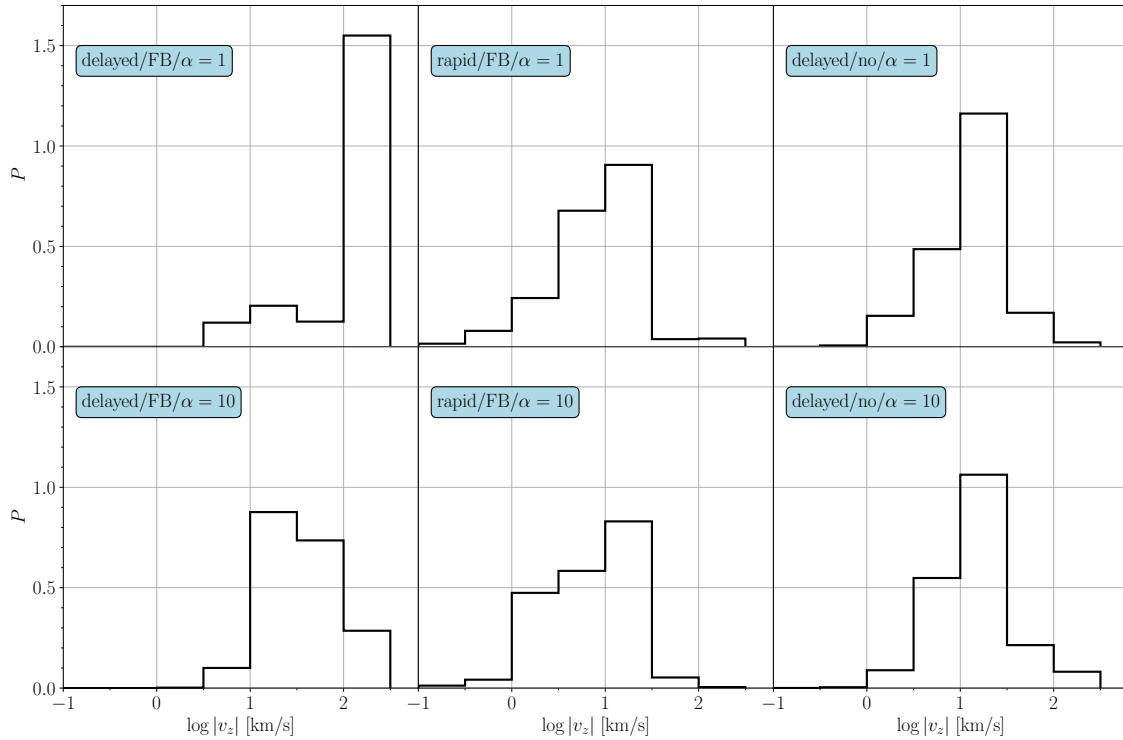


**Figure 7.** Probability density function of  $|v_z|$  of the detectable BH-LC binaries with different choices of the SN/kick models and values of the CE efficiency  $\alpha$ .

D.T. is supported by the Sherman Fairchild Postdoctoral Fellowship at Caltech. This research is supported by Grants-in-Aid for Scientific Research (17H06360, 19K03907, 22K03686) from the Japan Society for the Promotion of Science.

## APPENDIX

### A. CORNER PLOTS OF BINARY PARAMETERS

In this appendix, Figures 8 to 13 show two-dimensional scatter plots with binary parameters (BH mass  $m_{\text{BH}}$ , LC mass  $m_{\text{LC}}$ , orbital periods  $P$ , and eccentricities  $e$ ), spatial parameters (velocities in  $z$ -direction  $|v_z|$ , and the heights from the Galactic plane  $|z|$ ) and metallicity, and one-dimensional histograms for each choice of SN/kick models and  $\alpha$  values. Note that the vertical axis in the histograms is linear. Each point shows a BH-LC sample obtained from the 10 different realizations. The black point depicts the detectable BH-LC binaries. The blue ones are the entire Galactic BH-LC binaries with orbital period of 50 days to 10 years.

## REFERENCES

- Abbott, R., Abbott, T. D., Abraham, S., et al. 2020, *ApJL*, 896, L44
- Andrews, J. J., Breivik, K., & Chatterjee, S. 2019, *ApJ*, 886, 68
- Andrews, J. J., Taggart, K., & Foley, R. 2022, arXiv e-prints, arXiv:2207.00680
- Bailyn, C. D., Jain, R. K., Coppi, P., & Orosz, J. A. 1998, *ApJ*, 499, 367
- Belczynski, K., Bulik, T., Fryer, C. L., et al. 2010, *ApJ*, 714, 1217
- Bertelli, G., Bressan, A., Chiosi, C., Fagotto, F., & Nasi, E. 1994, *A&AS*, 106, 275
- Blaauw, A. 1961, *BAN*, 15, 265
- Bovy, J., Leung, H. W., Hunt, J. A. S., et al. 2019, *Monthly Notices of the Royal Astronomical Society*, 490, 4740. <https://doi.org/10.1093/mnras/stz2891>

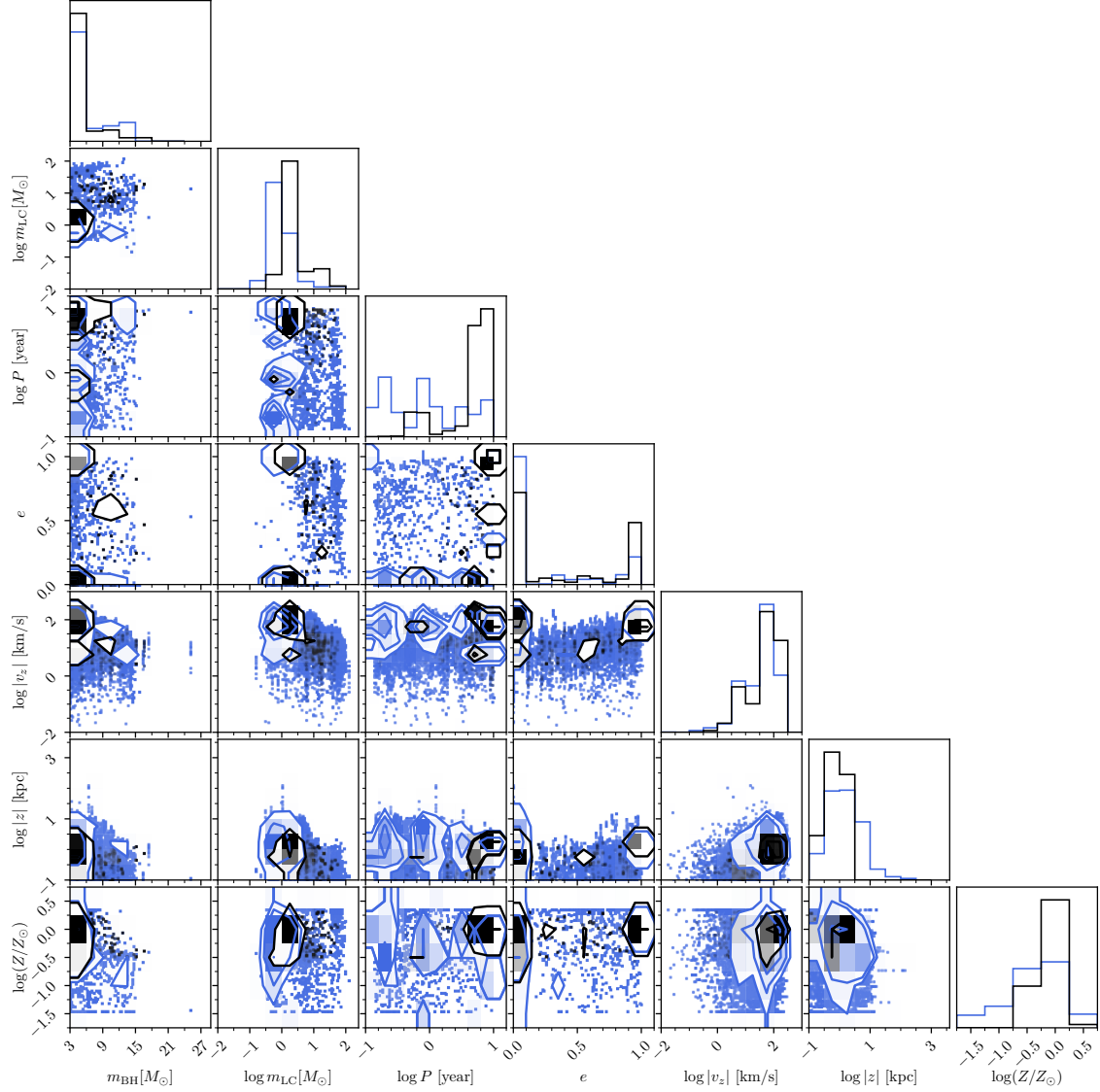


**Figure 8.** Corner plot of the current binary parameters (BH mass  $m_{\text{BH}}$ , LC mass  $m_{\text{LC}}$ , orbital periods  $P$ , and eccentricities  $e$ ), the current spatial parameters (velocities in  $z$ -direction  $|v_z|$ , and the heights from the Galactic plane  $|z|$ ), and metallicity  $Z/Z_{\odot}$  with the delayed SN model including FB kick and  $\alpha = 1$ . Histograms show the distribution of each parameter. The black lines and contours show the distributions of the detectable BH-LC binaries. The blue ones correspond to the Galactic BH-LC binaries within a period range,  $P = 50$  days to 10 years.

Breivik, K., Chatterjee, S., & Larson, S. L. 2017, *ApJL*, 850, L13

Chakrabarti, S., Simon, J. D., Craig, P. A., et al. 2022, arXiv e-prints, arXiv:2210.05003

Chawla, C., Chatterjee, S., Breivik, K., et al. 2021, arXiv e-prints, arXiv:2110.05979

Claeys, J. S. W., Pols, O. R., Izzard, R. G., Vink, J., & Verbunt, F. W. M. 2014, *A&A*, 563, A83

El-Badry, K., & Rix, H.-W. 2022, *MNRAS*, 515, 1266

El-Badry, K., Rix, H.-W., Quataert, E., et al. 2023, *MNRAS*, 518, 1057

Esa, . 1997, *VizieR Online Data Catalog*, I/239

Farr, W. M., Sravan, N., Cantrell, A., et al. 2011, *ApJ*, 741, 103

Frankel, N., Rix, H.-W., Ting, Y.-S., Ness, M., & Hogg, D. W. 2018, *The Astrophysical Journal*, 865, 96. <https://doi.org/10.3847/1538-4357/aadba5>

Fryer, C. L., Belczynski, K., Wiktorowicz, G., et al. 2012, *ApJ*, 749, 91

Gaia Collaboration, Prusti, T., de Bruijne, J. H. J., et al. 2016, *A&A*, 595, A1

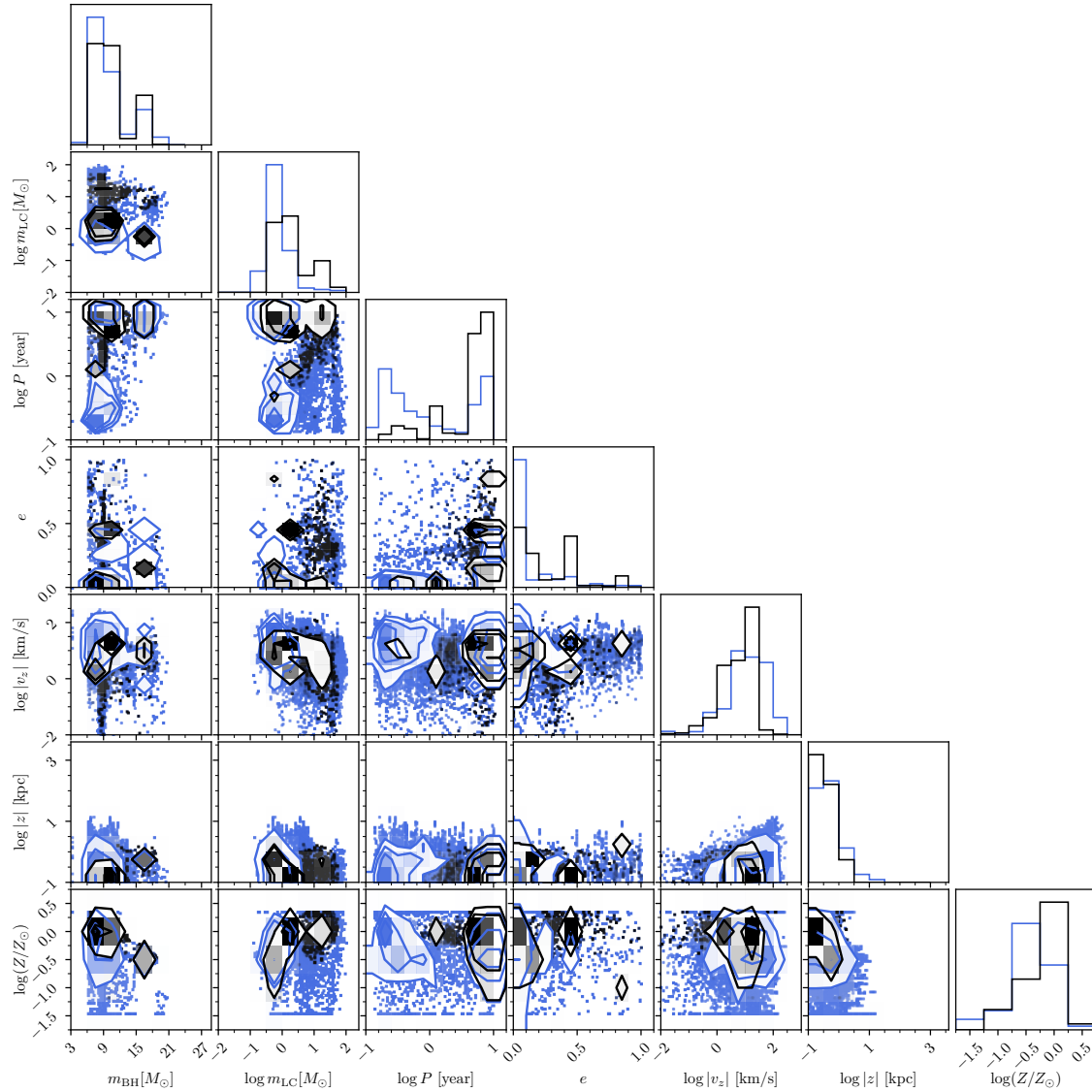


**Figure 9.** The same as Figure 8 except for the SN model. Here, the rapid SN model was employed.

Gaia Collaboration, Arenou, F., Babusiaux, C., et al. 2022, arXiv e-prints, arXiv:2206.05595

Gandhi, P., Rao, A., Charles, P. A., et al. 2020, MNRAS, 496, L22

Gandhi, P., Rao, A., Johnson, M. A. C., Paice, J. A., & Maccarone, T. J. 2019, MNRAS, 485, 2642

Gomel, R., Mazeh, T., Faigler, S., et al. 2022, arXiv e-prints, arXiv:2206.06032

Heggie, D. C. 1975, MNRAS, 173, 729

Hirai, R., & Mandel, I. 2022, ApJL, 937, L42

Hobbs, G., Lorimer, D. R., Lyne, A. G., & Kramer, M. 2005, Monthly Notices of the Royal Astronomical Society, 360, 974.

<https://doi.org/10.1111/j.1365-2966.2005.09087.x>

Hurley, J. R., Pols, O. R., & Tout, C. A. 2000, Monthly Notices of the Royal Astronomical Society, 315, 543.

<https://doi.org/10.1046/j.1365-8711.2000.03426.x>

Hurley, J. R., Tout, C. A., & Pols, O. R. 2002, MNRAS, 329, 897

Irrgang, A., Wilcox, B., Tucker, E., & Schiefelbein, L. 2013, A&A, 549, A137

Ivanova, N., Justham, S., Chen, X., et al. 2013, A&A Rv, 21, 59

Jayasinghe, T., Rowan, D. M., Thompson, T. A., Kochanek, C. S., & Stanek, K. Z. 2022, arXiv e-prints, arXiv:2207.05086

Jonker, P. G., Kaur, K., Stone, N., & Torres, M. A. P. 2021, arXiv e-prints, arXiv:2104.03596

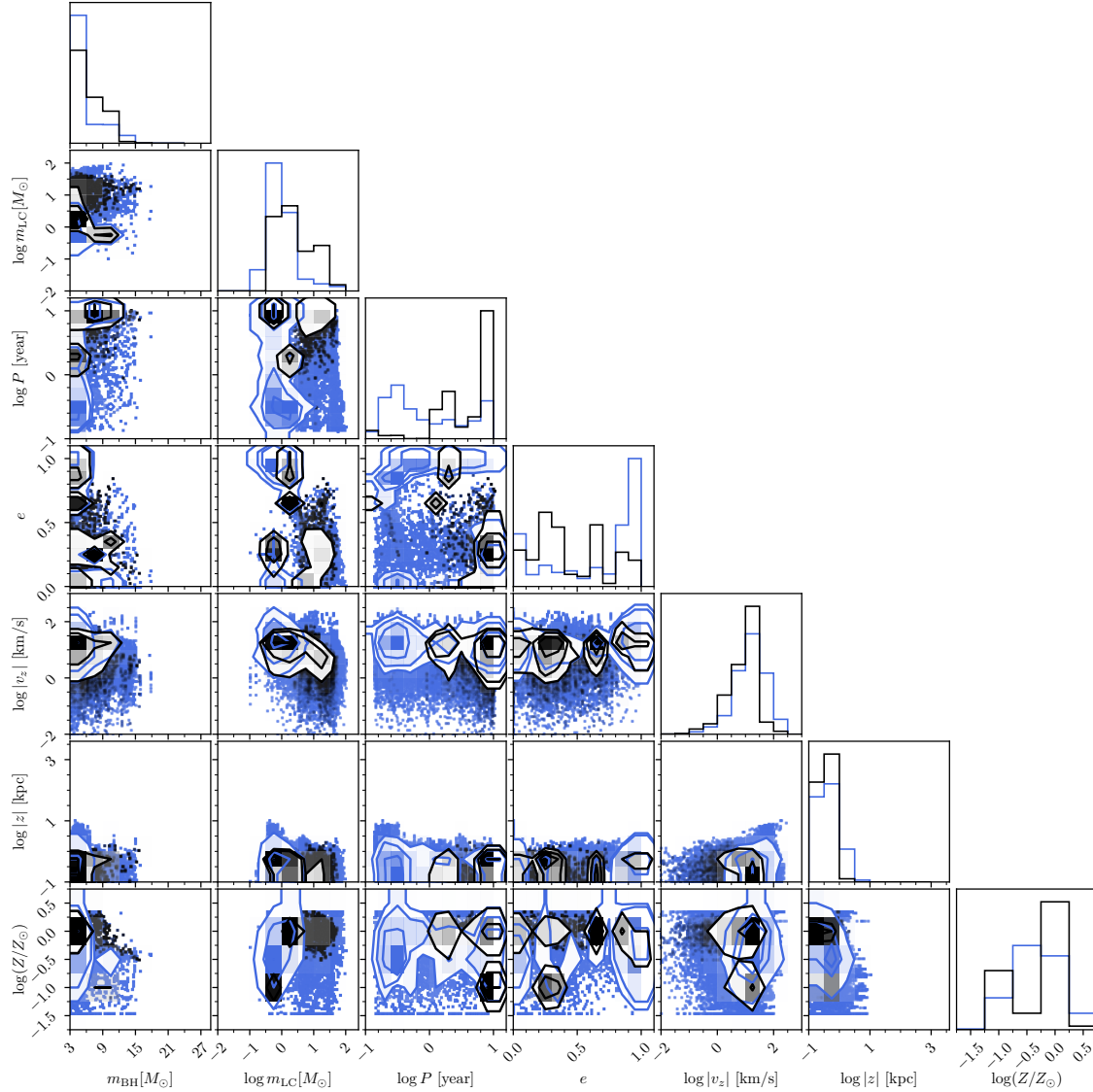


**Figure 10.** The same as Figure 8 except for kick model. Natal kick was excluded.

Jordi, C., Gebran, M., Carrasco, J. M., et al. 2010, *A&A*, 523, A48

Kinugawa, T., & Yamaguchi, M. S. 2018, arXiv e-prints, arXiv:1810.09721

Kobulnicky, H. A., & Fryer, C. L. 2007, *ApJ*, 670, 747

Kroupa, P. 2001, *Monthly Notices of the Royal Astronomical Society*, 322, 231. <https://doi.org/10.1046/j.1365-8711.2001.04022.x>

Kuiper, G. P. 1935, *PASP*, 47, 15

Licquia, T. C., & Newman, J. A. 2015, *The Astrophysical Journal*, 806, 96. <https://doi.org/10.1088/0004-637x/806/1/96>

Lucy, L. B. 2014, *A&A*, 563, A126

Majewski, S. R., Schiavon, R. P., Frinchaboy, P. M., et al. 2017, *The Astronomical Journal*, 154, 94. <https://doi.org/10.3847/1538-3881/aa784d>

Mashian, N., & Loeb, A. 2017, *MNRAS*, 470, 2611

McMillan, P. J. 2011, *Monthly Notices of the Royal Astronomical Society*, 414, 2446. <https://doi.org/10.1111/j.1365-2966.2011.18564.x>

O’Neil, K. K., Martinez, G. D., Hees, A., et al. 2019, *AJ*, 158, 4

Özel, F., Psaltis, D., Narayan, R., & McClintock, J. E. 2010, *ApJ*, 725, 1918

Sana, H., de Mink, S. E., de Koter, A., et al. 2012, *Science*, 337, 444

Shafter, A. W. 2017, *ApJ*, 834, 196

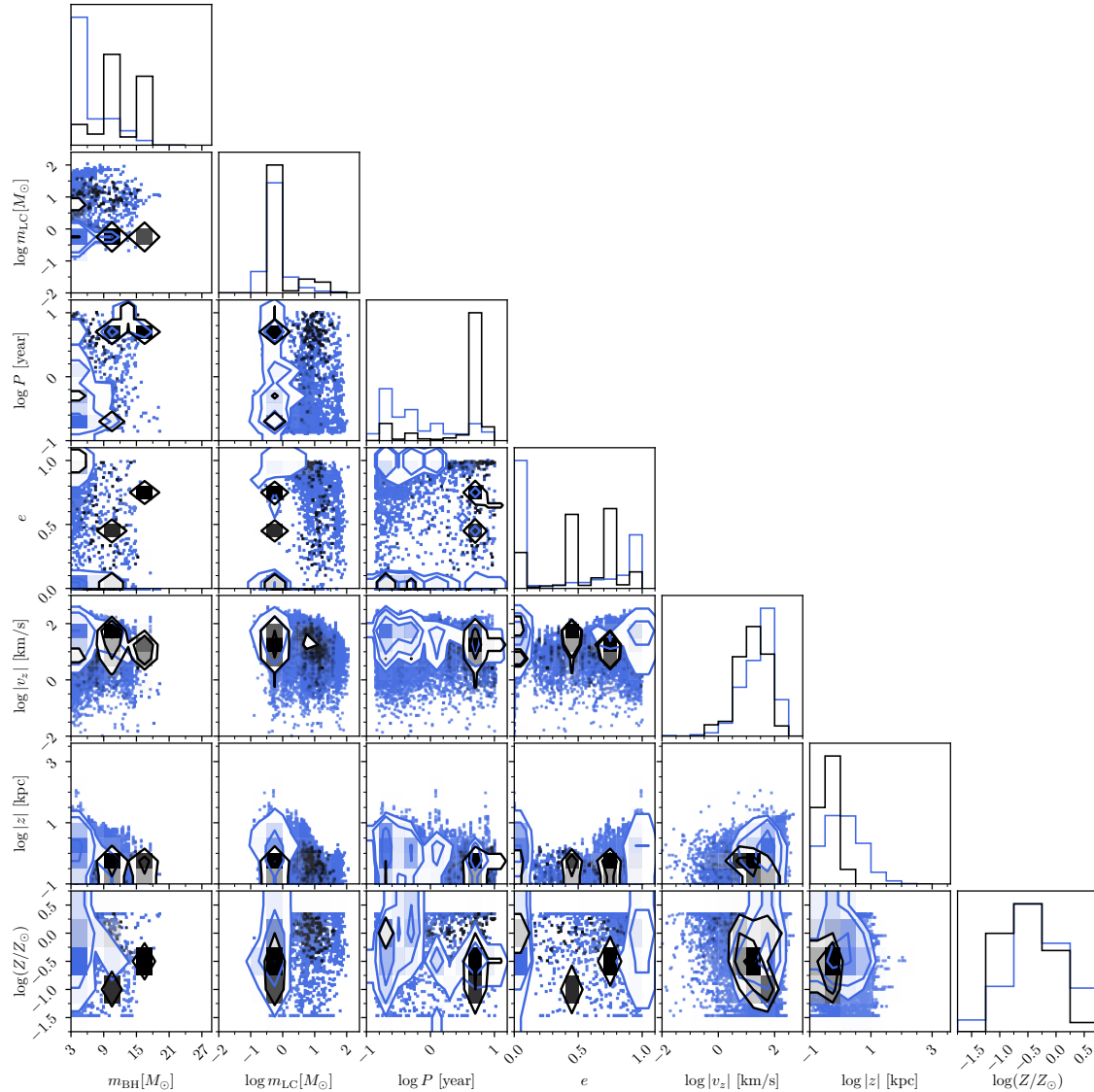


**Figure 11.** The same as Figure 8 except for the CE efficiency. Here, we adopted  $\alpha = 10$ .

Shahaf, S., Bashi, D., Mazeh, T., et al. 2022, MNRAS, arXiv:2209.00828

Shahaf, S., Mazeh, T., Faigler, S., & Holl, B. 2019, MNRAS, 487, 5610

Shao, Y., & Li, X.-D. 2019, ApJ, 885, 151

Shikauchi, M., Kumamoto, J., Tanikawa, A., & Fujii, M. S. 2020, PASJ, 72, 45

Shikauchi, M., Tanikawa, A., & Kawanaka, N. 2022, ApJ, 928, 13

Snaith, O. N., Haywood, M., Matteo, P. D., et al. 2014, The Astrophysical Journal, 781, L31.

<https://doi.org/10.1088/2041-8205/781/2/L31>

Spitzer, L. 1978, Physical processes in the interstellar medium, doi:10.1002/9783527617722

Sukhbold, T., Woosley, S. E., & Heger, A. 2018, ApJ, 860, 93

Tanikawa, A., Hattori, K., Kawanaka, N., et al. 2022, arXiv e-prints, arXiv:2209.05632

Tetzlaff, N., Neuhäuser, R., & Hohle, M. M. 2011, MNRAS, 410, 190

Torres, G. 2010, The Astronomical Journal, 140, 1158–1162. <http://dx.doi.org/10.1088/0004-6256/140/5/1158>

Tsuna, D., Kawanaka, N., & Totani, T. 2018, MNRAS, 477, 791

Wagg, T., Broekgaarden, F. S., de Mink, S. E., et al. 2021, arXiv e-prints, arXiv:2111.13704

Wegg, C., Gerhard, O., & Portail, M. 2015, Monthly Notices of the Royal Astronomical Society, 450, 4050.

<https://doi.org/10.1093/mnras/stv745>

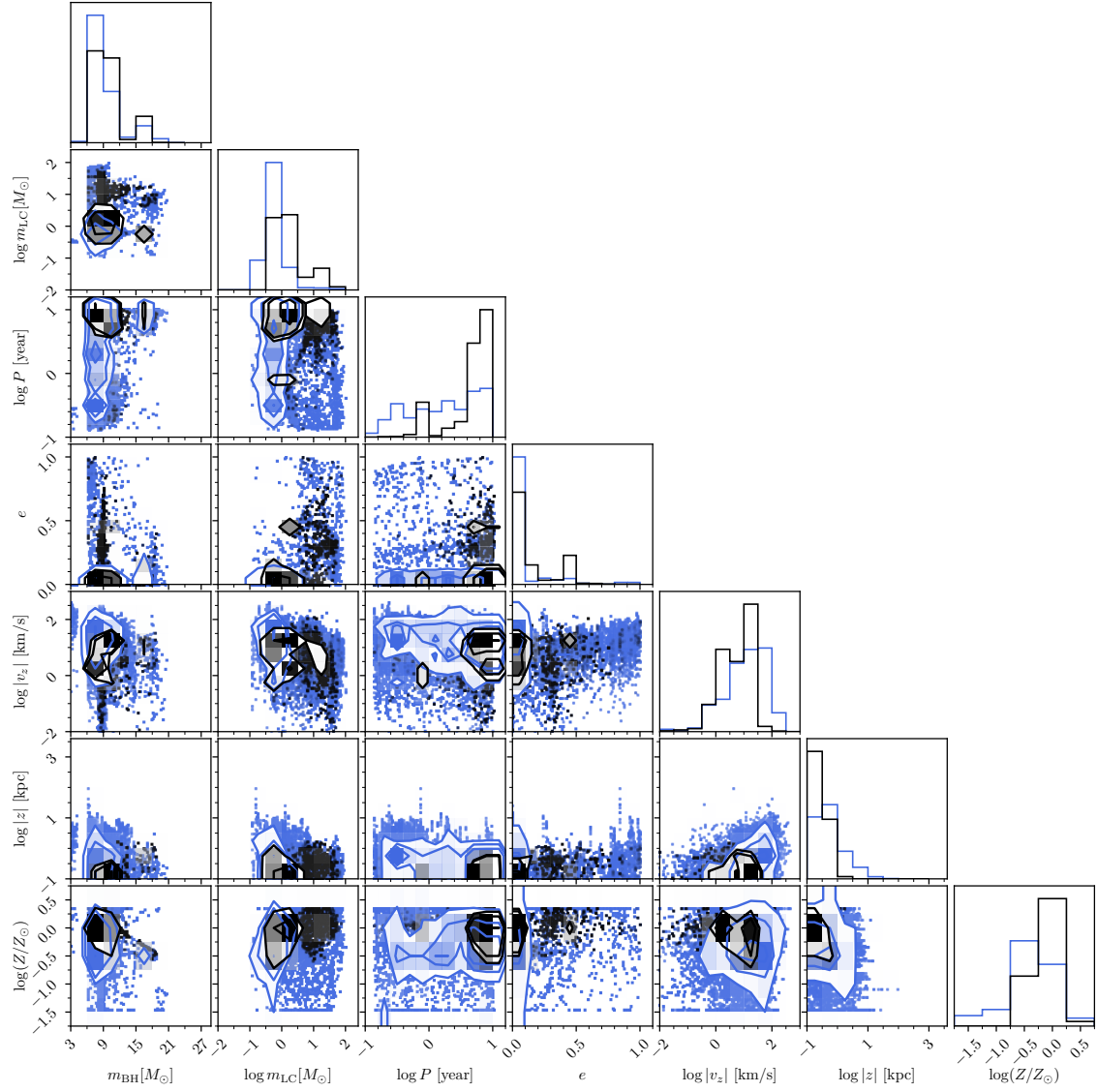


**Figure 12.** The same as Figure 9 except for the CE efficiency. Here, we adopted  $\alpha = 10$ .

Wiktorowicz, G., Lu, Y., Wyrzykowski, L., et al. 2020,

ApJ, 905, 134

Yalinewich, A., Beniamini, P., Hotokezaka, K., & Zhu, W.  
2018, MNRAS, 481, 930

Yamaguchi, M. S., Kawanaka, N., Bulik, T., & Piran, T.  
2018, ApJ, 861, 21

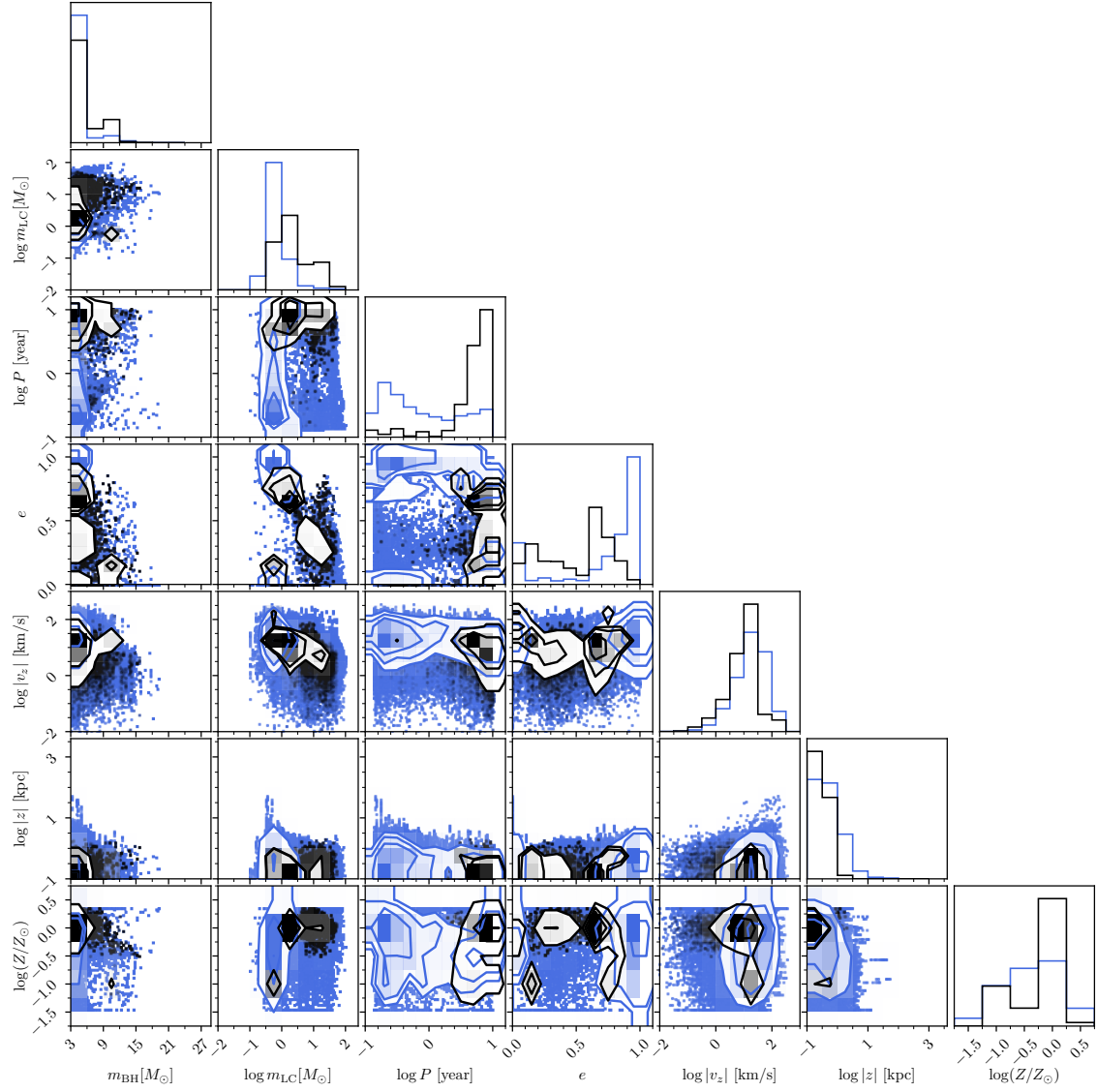


**Figure 13.** The same as Figure 10 except for the CE efficiency. Here, we adopted  $\alpha = 10$ .